


Ionospheric Research
NASA Grant No. NsG 134-61
Scientific Report
on
"Presunrise Effects Due to
Conjugate Region Photoelectrons"
by
M. W. Kwei
August 1, 1967
Scientific Report 301
Ionosphere Research Laboratory

Submitted by:



John S. Nisbet, Associate Professor of
Electrical Engineering, Project Supervisor

Approved by:



A. H. Waynick, Director, Ionosphere Research
Laboratory

The Pennsylvania State University
College of Engineering
Department of Electrical Engineering

ABSTRACT

In winter, as has previously been reported, the electron temperature at Arecibo starts to increase prior to local sunrise following illumination of the conjugate ionosphere. At this time an increase is also noticed in the 6300 Å airglow intensity. While both these effects have been attributed to photoelectron excitation from the conjugate hemisphere, a theory which would allow quantitative prediction of these two effects has hitherto been lacking.

Photoelectron fluxes calculated in the manner described by Nisbet (1967) have been used to examine the mechanism of pre-sunrise heating at Arecibo. Detailed analyses are made of the escaping photoelectron flux from the conjugate region including the effect of elastic collisions with neutrals in confining the photoelectrons. Comparisons between the theoretical heat input and observed energy losses in ambient electrons are presented. Also the theoretical and measured heat fluxes are compared.

Calculations have been made of the enhancement in intensity of the 6300 Å airglow and these results are compared with measurement at Haute Provence. In this way a comparison has been made which shows that the direct excitation of the airglow by the photoelectrons as proposed by Carlson (1966) predominates over excitation by the heated ambient electrons as proposed by Cole (1965).

TABLE OF CONTENTS

	Page
Abstract	ii
Table of Contents	iii
1. INTRODUCTION	1
1.1 General Statement of the Problem	1
1.2 Previous Related Studies	4
1.2.1 Evidence From Oxygen Red Line Measurements	4
1.2.2 Evidence From Backscatter Measurements	5
1.2.3 Theoretical Considerations	7
1.3 Specific Statement of the Problem	12
2. PRODUCTION OF IONIZATION	13
2.1 Introduction	13
2.2 Solar Ionizing Radiation, Ionization and Absorption Cross Sections	14
2.3 Model Atmosphere	14
2.4 Height Profiles and Energy Spectrum of Production Rates of Photoelectrons	15
3. RATES OF ENERGY LOSS OF PHOTOELECTRONS	19
3.1 Losses to Neutral Particles	19
3.1.1 Elastic Collisions	19
3.1.2 Inelastic Collisions	19
a. Basic Equations	19
b. Inelastic Collision Cross-Sections	20
c. Results of Calculations	23
3.2 Losses to Ions	23

	Page	
3.3	Losses to Ambient Electrons	28
	a. Basic Equation.	28
	b. Electron Density Profile.	28
	c. Results of Calculations	28
3.4	Total Time Rates of Energy Loss	31
4.	NUMBER DENSITY OF PHOTOELECTRONS	34
4.1	Probability of Escape of Photoelectron.	34
4.2	Continuity Equation for the Photoelectron Number Density.	39
4.3	Height Profile of Photoelectron Number Density	43
5.	UPWARD-GOING PHOTOELECTRON FLUXES.	48
5.1	Diffusion Flux of Photoelectrons.	48
5.2	Escape Flux of Photoelectrons	54
6.	ENERGY DEPOSITED IN THE PROTONOSPHERE AND THE DOWNWARD HEAT FLUX	56
6.1	Basic Equation.	56
6.2	Line Integral of the Electron Density Along the Field Line.	57
6.3	Results of Calculations	57
7.	HEAT INPUT TO THE AMBIENT ELECTRONS IN THE DARK IONOSPHERE DUE TO MAGNETIC CONJUGATE POINT PHOTOELECTRONS	62
8.	ENERGY-LOSS OF THE CONJUGATE POINT PHOTOELEC- TRONS DUE TO THE EXCITATION OF THE OXYGEN RED LINE IN THE DARK IONOSPHERE.	65
9.	ENERGY LOSSES OF AMBIENT ELECTRONS	68
9.1	Energy Loss Due to Excitation of ¹ D State of Atomic Oxygen.	68
9.2	Energy Loss Due to Other Inelastic Collisions with Neutral Particles	70
9.3	Energy Losses Due to Elastic Collisions with Neutral Particles and Positive Ions.	70

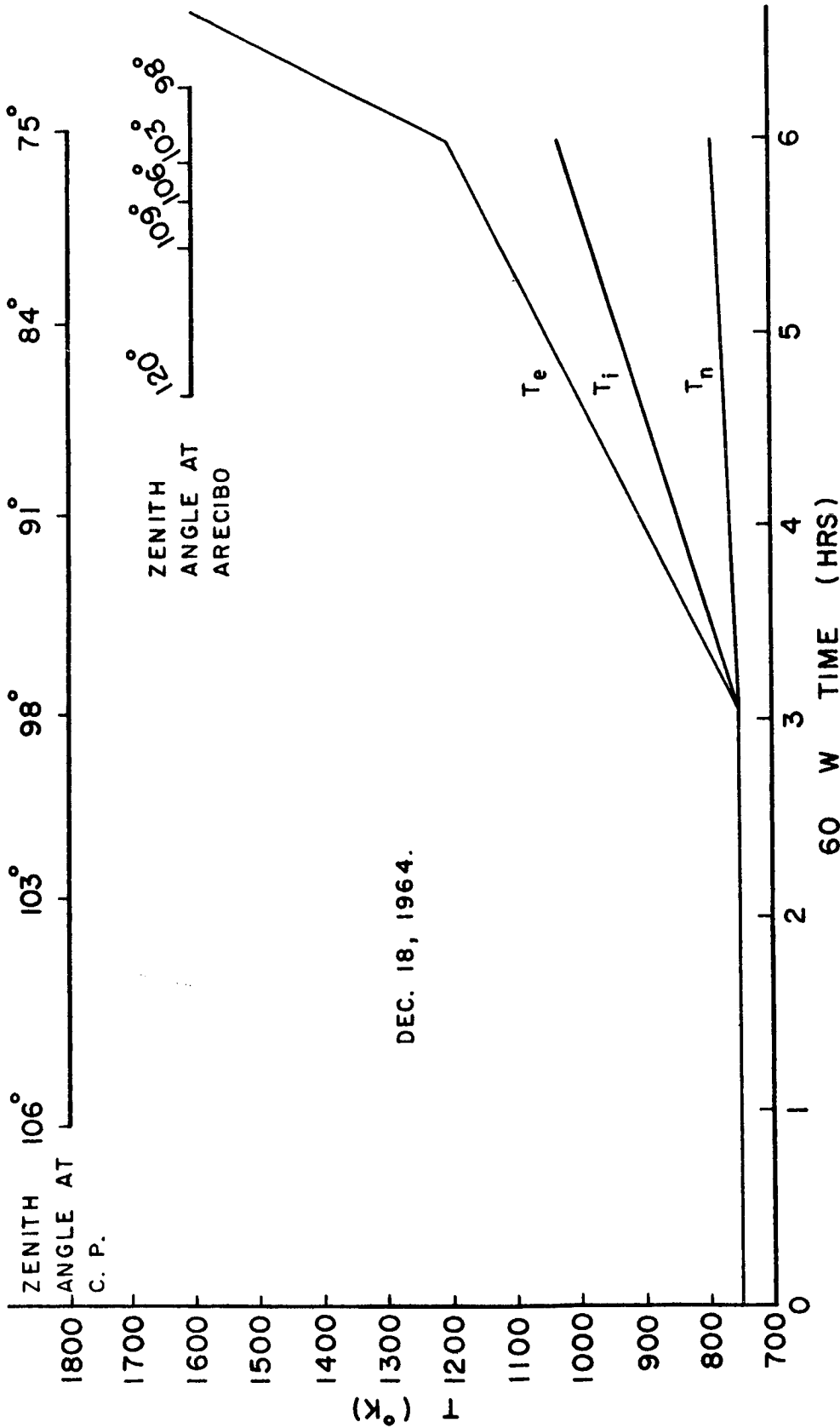
	Page
9.4 Height Profiles of Energy Losses of Ambient Electrons	71
10. THERMAL CONDUCTION	79
11. SUMMARY AND CONCLUSIONS.	80
11.1 Energy Distribution of Photoelectron Number Density	80
11.2 Diffusion Flux and Escape Flux of Photoelectrons	80
11.3 Energy Deposited in the Prontonosphere and the Downward Heat Flux	81
11.4 Heat Input and Energy-Loss of the Ambient Electrons in the Dark Ionosphere Above Arecibo	82
11.5 Pre-dawn Enhancement of the Intensity of 6300 Å Airglow Red Line	82
11.6 Suggestions for Further Research	83
Bibliography	85
APPENDIX.	90
Acknowledgements.	96

1. INTRODUCTION

1.1 General Statement of the Problem

The pre-sunrise heating of the ambient electrons in the ionosphere was first noticed in a series of experiments performed at the Arecibo Ionospheric Observatory in Puerto Rico by Carlson and Nisbet (1965) in December 1964. Since then it has been discussed by Carlson (1966) using Arecibo data and by Carru, Petit and Waldteufel (1966) using data obtained at Saint-Santin de Maurs in France. The observations indicate an increase in the electron temperature during the pre-dawn period in the ionosphere above an altitude which varies with latitude and solar cycle. Under low sunspot conditions at Arecibo, this altitude is about 300 Km. Fig. 1 shows the electron temperature as a function of time at the 375 Km. level at Arecibo. It is obvious that the electron temperature at this altitude in the dark ionosphere above Arecibo starts to increase at about the time when the zenith angle in the conjugate region is about 98° . The electron temperature increases more rapidly after local sunrise.

During the presunrise period there is a gradient in the electron temperature in the upper ionosphere. This gradient persists throughout the day and corresponds to a heat flux of the order of $10^8 \text{ ev-cm}^{-2}\text{-sec}^{-1}$ in the predawn period and of the order of $10^9 \text{ ev-cm}^{-2}\text{-sec}^{-1}$ during the day.



ELECTRON TEMPERATURE, ION TEMPERATURE, AND NEUTRAL TEMPERATURE AT ARECIBO (375 Km) FIGURE 1

Barbier (1959) noticed that the intensity of the 6300 Å airglow line increased prior to local dawn and Cole (1965) suggested that this might be caused by photoelectrons from the conjugate region. Carlson (1967) has since shown that this effect is well correlated at Arecibo with the pre-sunrise electron temperature increase.

Any theory for the photoelectron heating of the conjugate region must explain quantitatively three pieces of data. The first is the observed heating of the F-region as a function of altitude and time. The second is the downward heat fluxes from the protonosphere, both during the pre-sunrise period and throughout the day. The third is the pre-dawn enhancement of the intensity of the oxygen red line at 6300 Å.

1.2 Previous Related Studies

1.2.1 Evidence from Oxygen Red Line Measurement

Based on the measurements by Barbier (1959) at Haute Provence ($43^{\circ} 56' N$, $5^{\circ} 43' E$), Cole (1965) suggested that backscattered photoelectrons from the sunlit conjugate ionosphere are responsible for a major contribution to the predawn enhancement of 6300 \AA nightglow, by raising the temperature of F-region electrons.

Using the measured value of about 100 Rayleighs (From Fig. 5 of Barbier's paper the intensity of the red line is about 150 Rayleighs during the predawn period near winter solstice in 1956 and 1957, about 100 Rayleighs in 1955, and about 50 Rayleighs in 1953.) emanated from an altitude of about 230 Km. above Haute Provence, Cole (1965) interpreted these data on the basis of the excitation of the red line by the ambient electrons heated by the incoming photoelectrons and arrived at estimates of the electron temperatures that would have been required. These calculations referred to medium solar activity and the required temperatures were much larger than were observed at Arecibo under solar minimum conditions. Cole did not, however, examine the relationship between energy losses of the incoming photoelectrons to the ambient electrons and the various neutral loss processes, a factor of major importance in the solution of this problem.

1.2.2 Evidence from Backscatter Measurements

Quinn and Nisbet (1963) investigated the recombination in the nighttime F-layer using Puerto Rico ionograms. In the course of this analysis it was found that the equivalent thickness of the F layer decreased more slowly during winter nights than in summer. It was suggested that the possible cause of this effect might be a difference in the behavior of electron temperature between winter and summer. The effect of such changes in electron temperature on the recombination coefficients was calculated. To investigate whether such effects did occur a series of experiments was run at Arecibo in the winter of 1964. It was found by Carlson and Nisbet (1965) that the electron temperatures at the 450 and 375 Km. level above Arecibo on December 18, 1964 decreased rather slowly until about midnight, while those at 225 Km. reduced quite rapidly after local sunset, and that the electron temperatures at all levels decreased rapidly to the nighttime value after local sunset on July 12, 1964.

Carlson and Nisbet (1965) pointed out that at about 02:30 hrs. (local time from their Fig. 1) on December 18, 1964 the electron temperature at 375 and 450 Km. above Arecibo started to increase quite rapidly even though local sunrise at these altitudes was not until about

05:20 hrs. and attributed them to conjugate point photo-electrons.

Evans (1965, 1967) has published extensive data on the electron and ion temperatures for Millstone Hill. Due to the greater latitude of the conjugate region and the large difference in longitude between Millstone and its conjugate region only for 60 days per year would the effect be noticeable. According to Evans (1967) the effect has been observed but for the above reasons it is not nearly as marked as it is at Arecibo or St. Santin de Maurs.

According to Carru, Petit, and Waldteufel (1966), the measurements made at Saint-Santin de Maurs ($L \sim 18$) between the altitudes of 200 and 400 Km. and between November 1965 and March 1966 also illustrate the heating of the ionosphere by photoelectrons from the magnetic conjugate point. Their results show that on January 25, 1966 the electron temperature begins to increase around three hours before ground sunrise at Saint-Santin, and that the start of this phenomena coincides well with the sunrise at the magnetic conjugate point of Saint-Santin. Their observations made on November 17, 1965; January 26, 1966; February 17, 1966; and March 2, 1966 confirm the above result.

Perkins and Salpeter (1965) have predicted that the presence of a small number of energetic electrons can enhance the intensity of the electron density fluctuations near the electron plasma frequency. The daytime enhancement has been observed (Perkins, Salpeter and Yngvesson, 1965) up to an altitude exceeding 400 Km. They also found some evidence of a predawn enhancement in a set of winter sunrise observations at Arecibo suggesting a flux of photoelectrons from the sunlit magnetic conjugate region.

1.2.3 Theoretical Considerations

Hanson and Johnson (1961) predicted that energetic electrons would share their energy more readily on colliding with other electrons than on colliding elastically with ions or neutral particles, due to the mass ratio, and that this makes it probable that the average electron energy would be higher than the average energy of ions and neutral particles; that is, the electron temperature would probably exceed the ion and neutral particle temperatures. They ignored the energy loss of photoelectrons due to the excitation of upper electronic states of molecular nitrogen because the cross sections for these excitation were not available to them.

They also pointed out that the excess energy of anagnet electrons must be transferred to the neutral and ion gas for conduction downward. Only if the electron temperature is of the order of $10,000^{\circ}$ K. or higher would conduction in the electron gas be important. Thus, in calculating the electron temperature they neglected the heat conduction of the ambient electrons.

Hanson (1963) was the first to point out that because of the long mean free path above 300 Km., the photoelectrons present above this level with sufficient energy have a high probability of escape to the outer ionosphere by spiraling along the magnetic field line and back to the ionosphere in the conjugate hemisphere.

Based on the model atmosphere chosen to match the time and place of the solar ultraviolet measurements (August 23, 1961, 10:04 AM, MST) made by Hall, Damon, and Hinteregger, Hanson estimated the altitude above which the photoelectron can escape upward without experiencing ionizing collision with the atomic oxygen to be about 280 Km. Considering the elastic collision of the photoelectron with atomic oxygen, he calculated the escape altitude to be about 350 Km. for one elastic collision, and about 285 Km. for three elastic collisions. He also pointed out that the effective escape altitude would be raised when magnetic dip angle and pitch angle of the photoelectron

are taken into account. Considering the confinement of the fast electrons by elastic collisions with the ambient electrons, he found that the photoelectron can escape if the local value of electron density is

$$n_e = 1.4 \times 10^4 E_0 \cos \theta_p \sin I$$

where E_0 is the initial energy of the photoelectron, θ_p is the pitch angle, and I is magnetic dip angle.

Hanson estimated the total flux of fast electrons to be 10^9 electrons-cm⁻²-sec⁻¹.

Dalgarno et al. (1963) calculated in detail the various energy losses of the photoelectrons. Having compared the efficiencies of energy loss to the neutral particles and to the ambient electron and assuming that the photoelectrons deposit their energy locally, they calculated the electron temperature as a function of altitude, ignoring the heat conduction of the electron gas.

Assuming negligible collisions between photoelectrons and neutral particles above 300 Km. and assuming the pitch angles of the photoelectrons not to be changed, Geisler and Bowhill (1965) developed a theory of non-local heating and derived the expressions for the heat input to the ambient electrons due to two photoelectron fluxes,

one from above and one from below.

They calculated the electron temperature height profile taking into account the thermal conduction of the ambient electrons for several different levels of solar activity.

Carlson (1966) has pointed out that the specific mechanism for the predawn enhancement of 6300 Å airglow proposed by Cole (1965) is excitation of the atomic oxygen 1D state by thermal electrons. Carlson felt that from his model direct excitation of the 1D state by incident photoelectrons seemed a more likely mechanism.

Carlson (1966), using photoelectron spectrum based on Mariani's data (1964) for solar zenith angle of 90° and following the calculations parallel to Perkins (1964), estimated the spectrum of photoelectrons escaping upwards from the 600 Km. altitude level of the conjugate ionosphere as follows:

$$\phi = 2.9 \times 10^7 \text{ cm}^{-2} \text{-sec}^{-1} \text{-ev}^{-1}, \text{ for } 30 \geq E \geq 10 \text{ ev.}$$

$$\phi = 0 \quad \text{for } E > 30 \text{ ev.}$$

$$\phi = \frac{E}{10} \times 2.9 \times 10^7 \quad \text{for } E < 10 \text{ ev.}$$

For these models he estimated the energy flux through the 600 Km. level to be $3 \times 10^8 \text{ ev-cm}^{-2} \text{-sec}^{-1}$.

Without considering the various energy loss processes of the photoelectrons before escape, Banks (1965) estimated the total photoelectron flux produced in the conjugate region to Arecibo in the early morning to be 7.3×10^7 electrons-cm⁻²-sec⁻¹. Then, assuming that a single collision with the neutral particles is adequate to localize a given incoming photoelectron and that only the scattered photoelectrons can transfer the energy to the ambient electrons in the ionosphere above Arecibo, he calculated the heat input to the ambient electrons without using the electron density. His height profile has a peak value of 13.5 ev-cm⁻³-sec⁻¹ at an altitude of 260 Km., and the heat input is about 9ev-cm⁻³-sec⁻¹ at 300 Km.

1.3 Specific Statement of the Problem

- (1) To investigate the photoelectron number densities in the conjugate ionosphere of Arecibo including the effect of escape of photoelectrons.
- (2) To investigate the escape mechanisms of photoelectrons and the factors controlling the escape component of the photoelectron flux at the various altitudes.
- (3) To examine the effect of traversing the field lines on the photoelectron flux and to calculate the heat flux conducted downwards into the ionosphere above Arecibo.
- (4) To calculate the effect of these incoming photoelectrons on the ionosphere above Arecibo and to compare the theoretical prediction with the observed heat input.
- (5) To calculate the predawn enhancement of the intensity of the 6300 ^oA airglow red line due to photoelectrons from the conjugate point and due to the high energy tail of the ambient electrons.

2. PRODUCTION OF IONIZATION

2.1 Introduction

In order to compare the theoretical and measured values of the energy transfer rate of the ambient electrons, the heat flux conducted downwards and the intensity of the 6300A oxygen red line during the predawn period, it is necessary to calculate the production rates of photoelectrons in the sunlit conjugate region at a particular time on a particular day.

The production function of the i th ion for a certain spectral range at a given altitude, h , may be written as:

$$q_{ih} = n_{ih} K_{Ii} \Phi_{\infty} e^{-\sum_i \tau_i} \quad (2.1.1)$$

where

n_i = number density of the i th constituent of the neutrals

K_{Ii} = ionization cross section for the i th constituent

Φ_{∞} = photon flux of the solar radiation at the top of the atmosphere

τ_i = optical depth (non-dimensional)

Detailed considerations for $\sum_i \tau_i$ are given in appendix.

The energy spectrum of the primary photoelectrons may be obtained in a way somewhat similar to that adopted by Tohmatsu et al. (1965). The relationship between the solar zenith angle and the time is governed by the

following equation (Mitra, 1952):

$$\cos \chi = \cos \delta \cos \psi \cos \zeta + \sin \delta \sin \zeta \quad (2.1.2)$$

where

χ = solar zenith angle

δ = solar declination (positive north)

ψ = local hour angle (positive before noon)

ζ = latitude of the place of observation (positive north)

The calculated solar zenith angles for both ends of the magnetic field line are shown in Fig. 1.

2.2 Solar Ionizing Radiation, Ionization and Absorption Cross Sections

The photo fluxes, absorption cross sections and photo-ionization cross sections published by Hinteregger et al. (1964) have been used in this work. The mean solar flux at 10.7 cm. in July 1963 corresponding to the above flux measurements was 76 and that in December 1964 corresponding to the Arecibo results used in the present analysis was 75.2. Because of the very similar solar activity levels no correction based on solar activity was considered necessary.

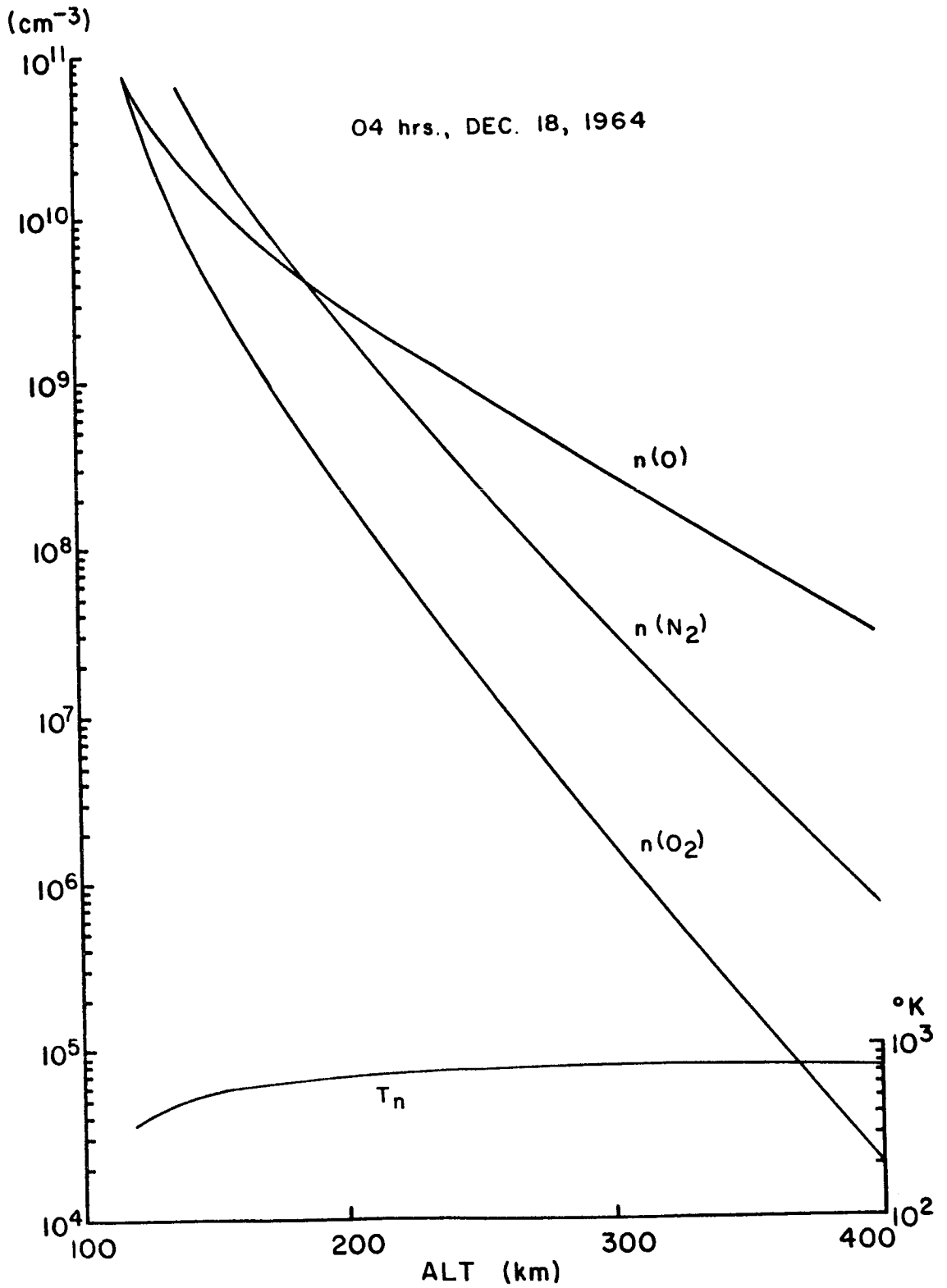
2.3 Model Atmosphere

The Cospar CIRA 1965 model atmosphere has been used throughout this work and necessary interpolation between models has been made in the manner described therein.

Fig. 2 shows the neutral densities and temperature for the interpolated model corresponding to 04 hrs. 60°W. time in the region of the conjugate point to the Arecibo Ionospheric Observatory.

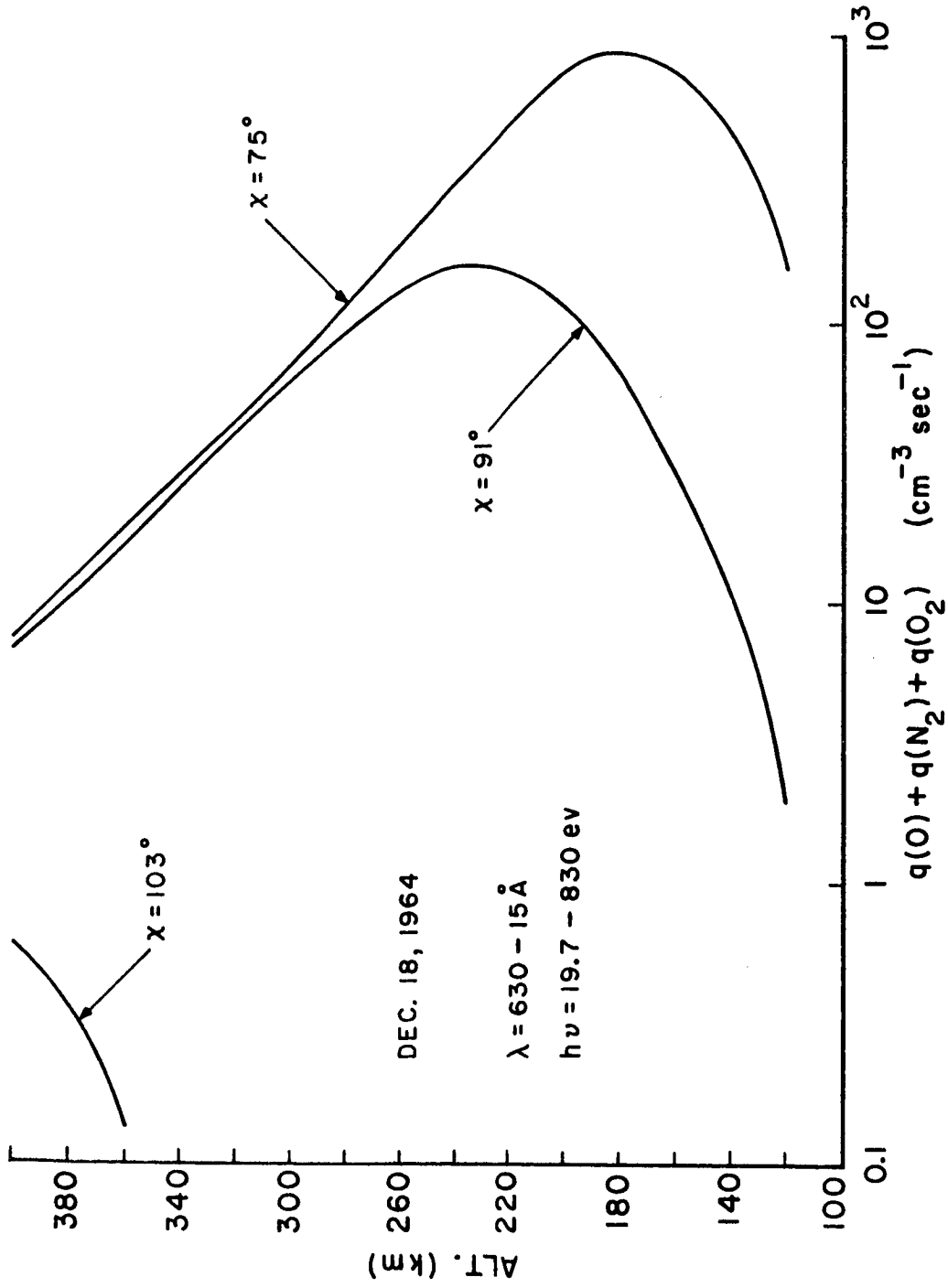
2.4 Height Profiles and Energy Spectrum of Production Rates of Photoelectrons

The production rates of photoelectrons have been calculated for each subgroup of the ionizing radiation, but only the total production rate is presented graphically in Fig. 3. At $\chi = 103^\circ$ (02:07 hrs. 60°W time) the production rate is less than one photoelectron $\text{cm}^{-3}\text{-sec}^{-1}$ below the 400-Km. level. This low production rate gives very little contribution to the heat input to ambient electrons in the dark ionosphere above Arecibo. This may be accounted for by the low and relatively constant value of electron temperature at the 375 Km. level at Arecibo as shown in Fig. 1. At $\chi = 91^\circ$ (04:04 hrs. 60°W time), the production rate reaches a value of 65 photoelectrons $\text{cm}^{-3}\text{-sec}^{-1}$ at 230 Km. At $\chi = 75^\circ$ (06:04 hrs. 60°W time) the production rate above 300 Km. is just a little higher than that at 04:04 hrs. but the peak production rate is somewhat larger and at a lower altitude (~ 180 Km.). The energy spectrum of production rates of photoelectrons at the 300 Km. level is shown in Fig. 4.



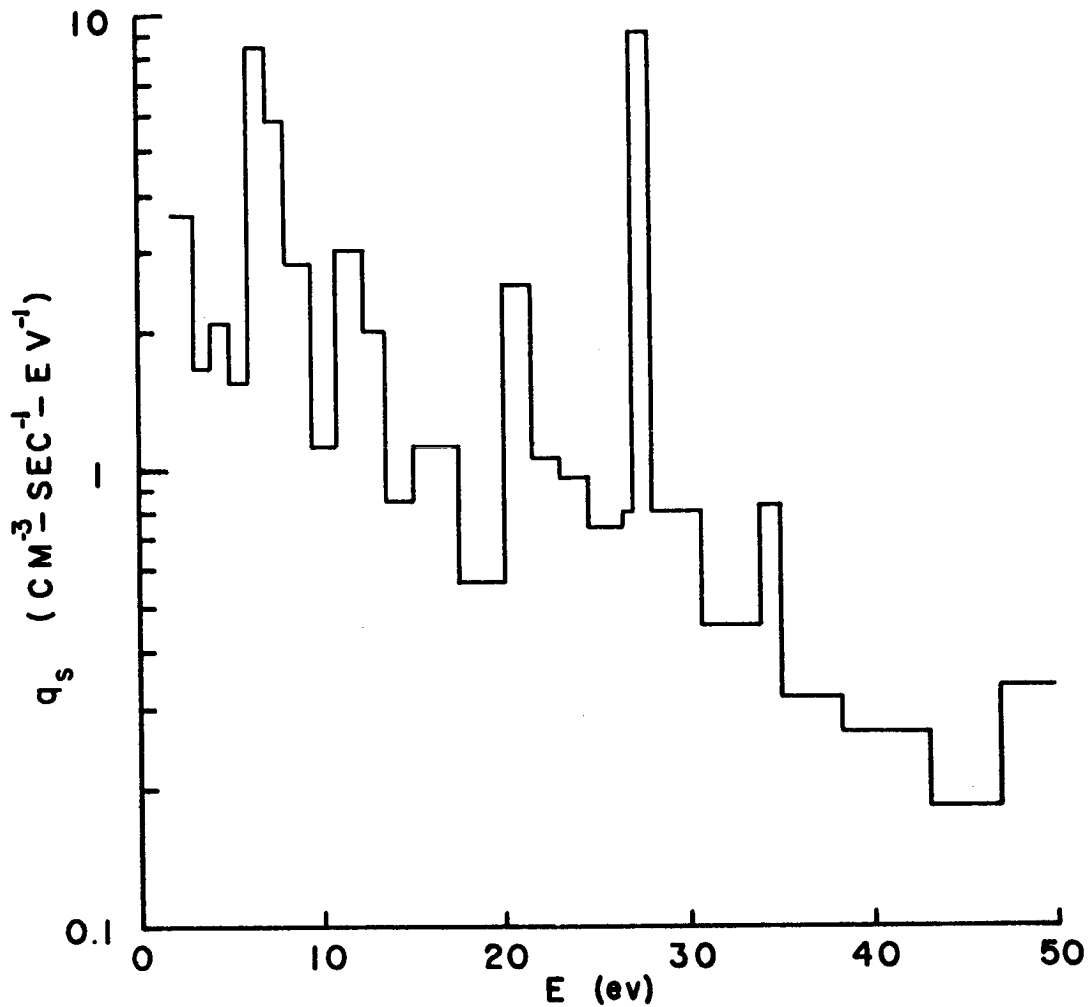
NUMBER DENSITIES AND TEMPERATURE OF NEUTRAL PARTICLES

FIGURE 2



TOTAL PRODUCTION RATES OF PHOTOELECTRONS IN THE CONJUGATE REGION

FIGURE 3



ENERGY SPECTRUM OF PRIMARY PHOTOELECTRONS (AT 300KM) IN CONJUGATE REGION $\chi = 91^\circ$

FIGURE 4

3. RATES OF ENERGY LOSS OF PHOTOELECTRONS

Having calculated the production rates of the photoelectrons, we must now examine the rates of energy loss of the photoelectron before we can calculate the photoelectron number densities.

3.1 Losses to Neutral Particles

3.1.1 Elastic Collisions

The rate of energy loss of photoelectrons through elastic collisions with neutral particles is given by (Dalgarno et al. 1963)

$$\frac{dE}{dx} = - \frac{2M_e}{M} nE\sigma_m \quad (3.1.1.1)$$

where M_e is the mass of an electron, M is the mass of the neutral particle, n is the number density of the air, and σ_m is the cross section for momentum transfer. The photoelectron loses little energy in an elastic collision with the neutrals because of the small mass ratio, but the angle of scattering may be large and control the diffusion velocity of the photoelectron.

3.1.2 Inelastic Collisions

a. Basic Equation

The basic equation used for the calculations of spatial rate of energy loss of a photoelectron is given by

$$\frac{dE}{dx} = -\sum_j \frac{A_j}{\lambda_j} = -\sum_j A_j n_j \sigma_j \quad (3.1.2.1)$$

where n_j is the number density of the j th constituent of

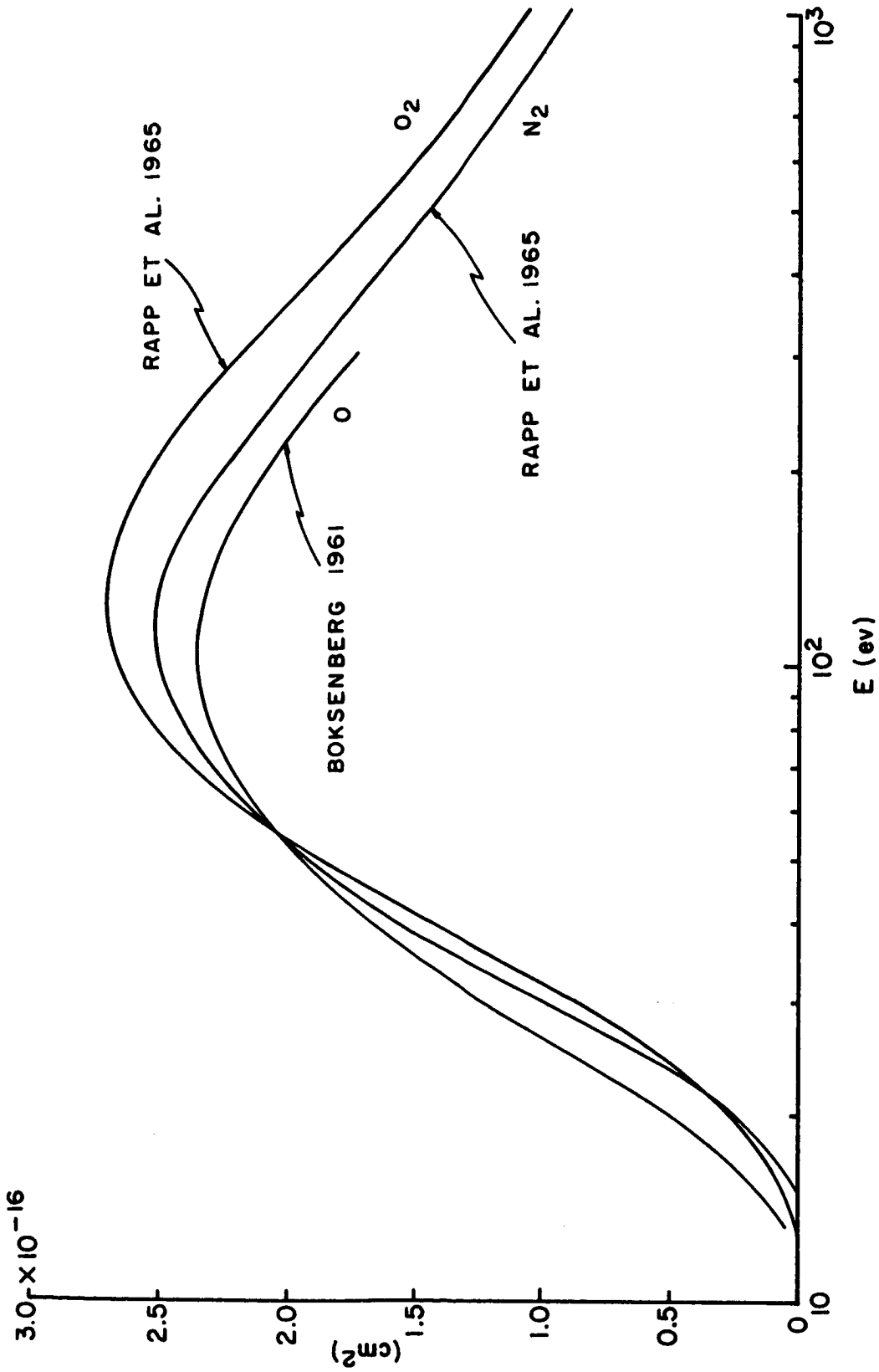
the neutral particles, σ_j is the cross section for the electron impact ionization or excitation of the j th constituent of the atmospheric gases, and A_j is the energy loss of the j th constituent of the neutrals for each ionizing or exciting collision. λ_j is the mean free path of a photoelectron for inelastic collisions with the j th constituent.

McDaniel (1964) has pointed out that if the energy of the incident electron is less than a few times the threshold energy for ionization of the target atom or molecule, all of the ejected electrons have energies of no more than a few ev. As the incident energy is increased, some secondaries of higher energy are produced. The great majority of photoelectrons produced by solar radiation have energies less than 70 ev. Following Dalgarno et al., (1963) we assume that for incident energies greater than 50 ev. the mean energy loss for each ionizing collision is 20 ev. For energies between 50 ev. and 20 ev., the mean energy loss in each ionizing process is 15 ev. For various excitation processes the energy loss in each collision is the threshold energy.

b. Inelastic Collision Cross Sections

For ionization cross sections we adopt those obtained by Boksenberg (1961) and Rapp et al. (1965) as shown in Fig. 5.

For excitations to the metastable 1D state of atomic oxygen, the cross sections calculated by Seaton (1956) as shown in Fig. 6, have been employed.



CROSS SECTIONS FOR IONIZATION BY ELECTRON IMPACT

FIGURE 5



CROSS SECTIONS FOR THE EXCITATION OF METASTABLE LEVELS OF ATOMIC OXYGEN BY ELECTRON IMPACT COMPUTED FROM THE RESULTS OF SEATON (1956)

FIGURE 6

Excitation to excited electronic levels of molecular oxygen (Schulz and Dowell 1962) is small in comparison and can be ignored at altitudes above 120 Km.

The cross sections for excitation of the first negative system of molecular nitrogen by electron impact measured by Stewart (1956) and that of the second positive system of molecular nitrogen by electron impact measured by Stewart and Gabathuler (1958) are about two orders of magnitude smaller than the ionization cross sections of O, O₂, and N₂, so they will not be considered here.

The cross sections for vibrational excitation and electronic excitation for electrons in molecular nitrogen obtained by Engelhardt et al. (1964) have been employed (Fig. 7).

c. Results of Calculations

The calculated spatial rates of energy loss of a photoelectron due to interaction with neutral particles as a function of electron energy are shown in Fig. 8. The magnitudes are comparable to those obtained by Hoegy et al. (1965) up to about 15 ev. and 300 Km.

3.2 Losses to Ions

The energy lost by photoelectrons in elastic collisions with ambient electrons is always large compared to that in elastic collisions with the ambient ions. According to Banks (1966) the rate of energy transfer from a photoelectron of energy E with $E \gg \frac{3}{2} kT_1$ to the ambient ions

is given by

$$\frac{dE}{dt} = \frac{4.2 \times 10^{-7} n_i \log \Lambda}{A_i E^{\frac{1}{2}}} \text{ ev-sec}^{-1} \quad (3.2.1)$$

and to ambient electrons as

$$\frac{dE}{dt} = \frac{7.7 \times 10^{-6} n_e \log \Lambda}{E^{\frac{1}{2}}} \text{ ev-sec}^{-1} \quad (3.2.2)$$

where A_i is the ion mass in atomic mass units ,

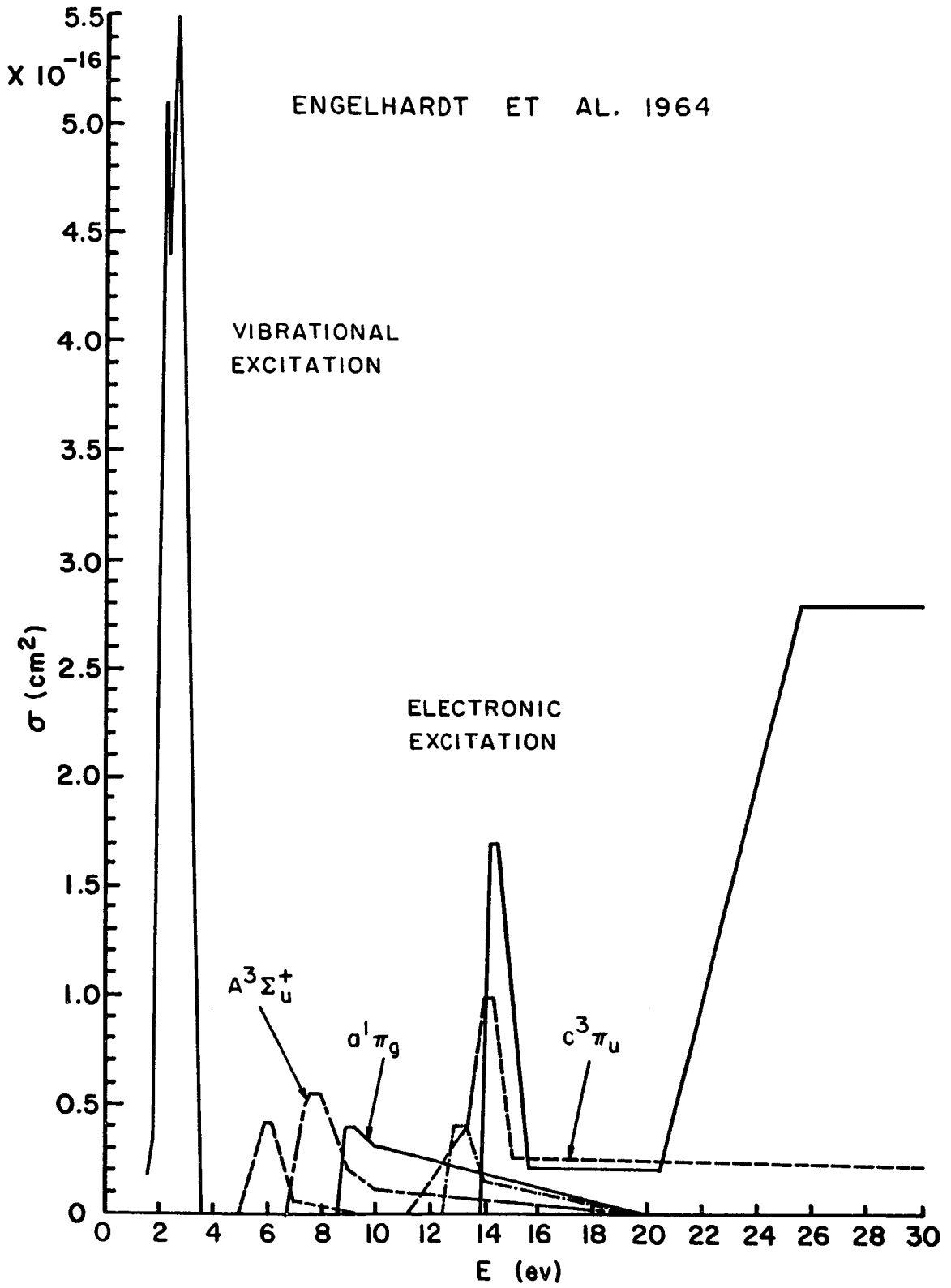
$$\Lambda = \frac{2E\lambda}{q}$$

q is the electronic charge and

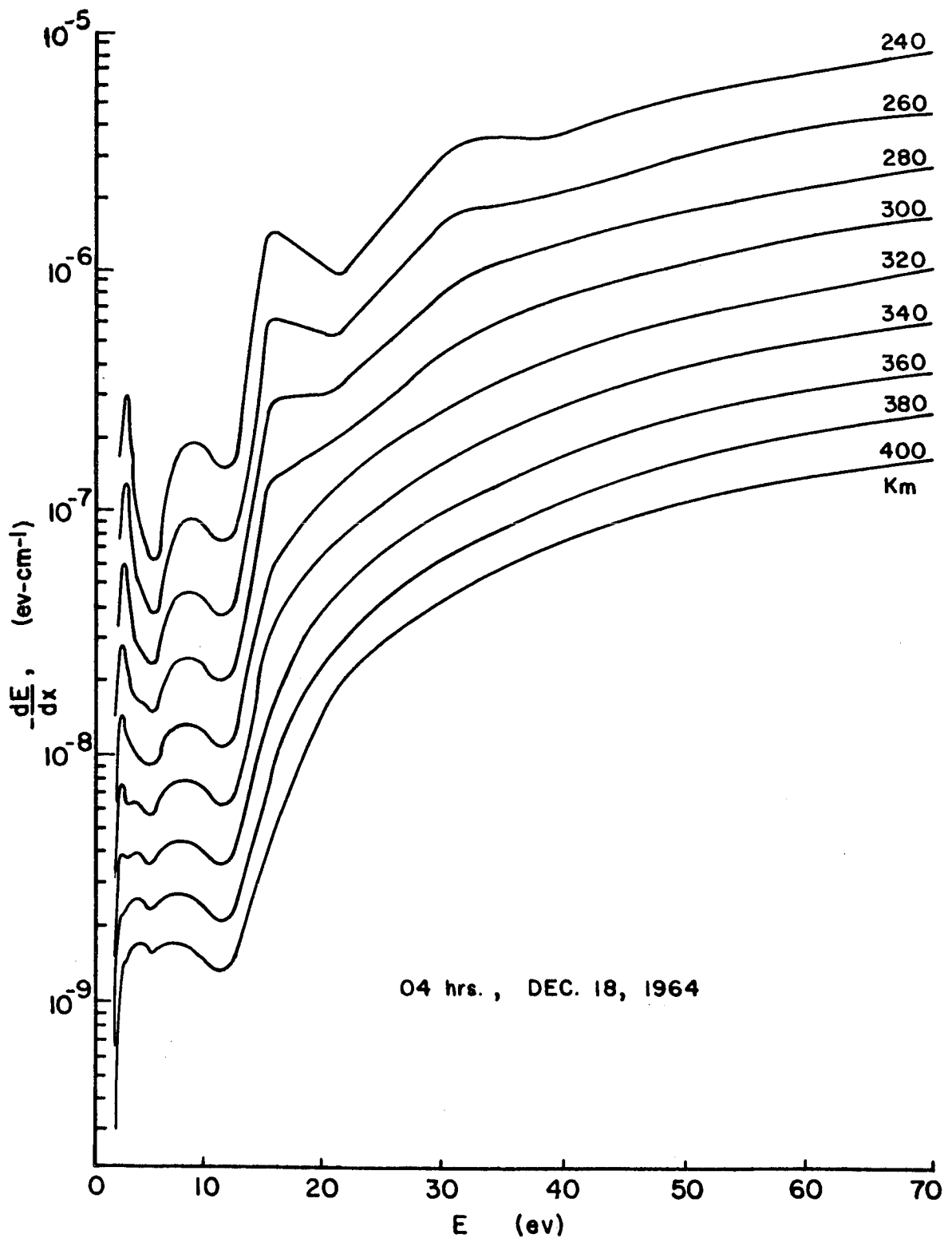
λ is the Debye length.

From Equations (3.2.1) and (3.2.2) we can see that the ratio of the heat given by the photoelectron to the ambient electrons to that given to the ambient ions will be $18.3 A_i$. The heating of atomic oxygen ions by photoelectrons is thus less effective by a factor of 293 at all energy levels than the heating of the ambient electrons.

Considering the inelastic collision of photoelectrons with the ions, the ion density is small in comparison with the neutral density. Thus, ions are not important at all in thermalizing the photoelectrons.

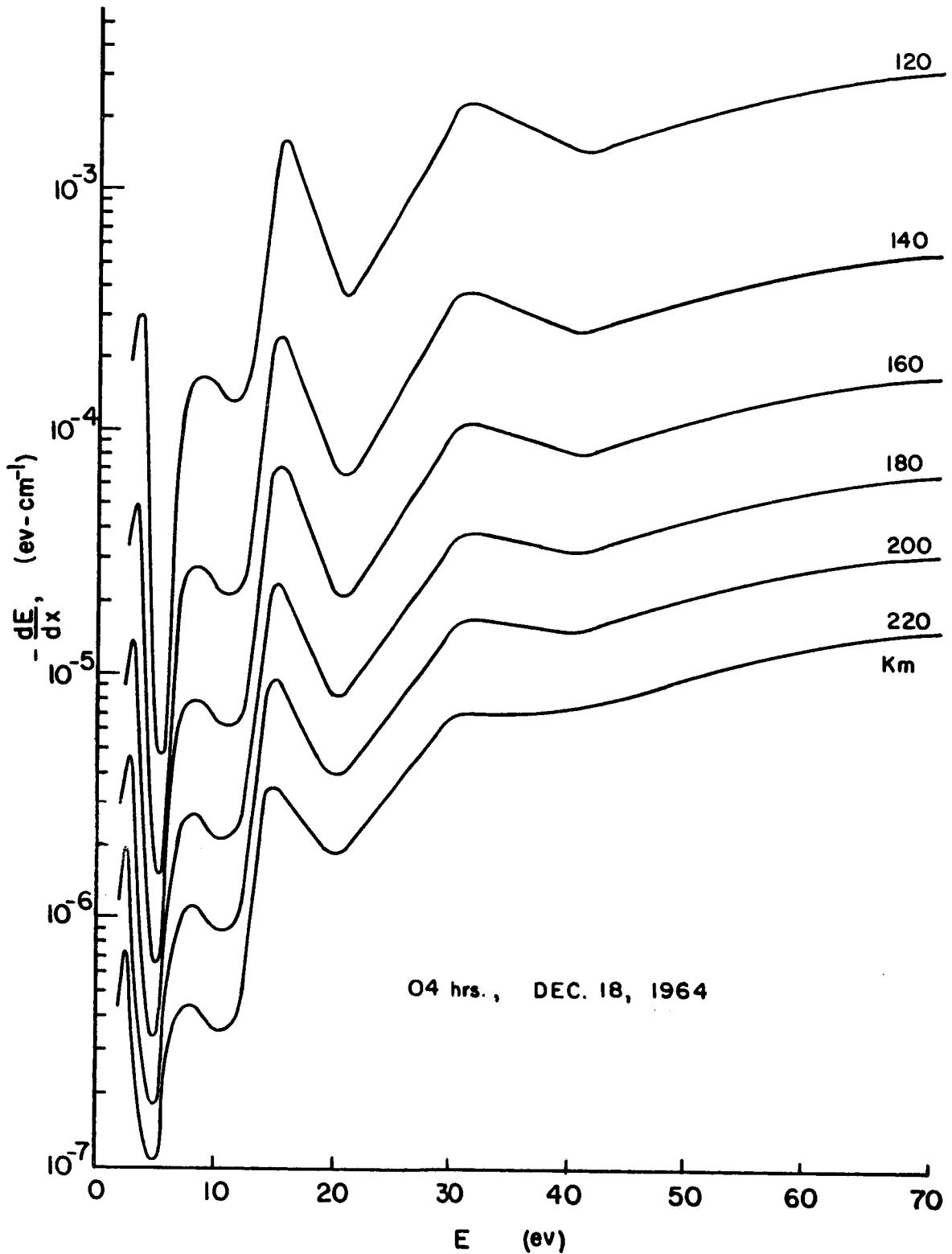


CROSS SECTIONS FOR VIBRATIONAL EXCITATION AND ELECTRONIC EXCITATION FOR ELECTRONS IN N_2
FIGURE 7



RATES OF ENERGY LOSS OF PHOTOELECTRON TO
NEUTRAL PARTICLES IN CONJUGATE REGION

FIGURE 8 (a)



RATES OF ENERGY LOSS OF PHOTOELECTRON TO
NEUTRAL PARTICLES IN CONJUGATE REGION
FIGURE 8 (b)

3.3 Losses to Ambient Electrons

a. Basic Equation

An expression for the rate of energy loss of a photoelectron through elastic collisions with the ambient electrons has been developed by Butler and Buckingham (1962). For energies greater than 3 ev, it is permissible to use the asymptotic form of this expression: (Dalgarno, et al., 1963)

$$\frac{dE}{dx} = - \frac{1.95 \times 10^{-12} n_e}{E} \quad (3.3.1)$$

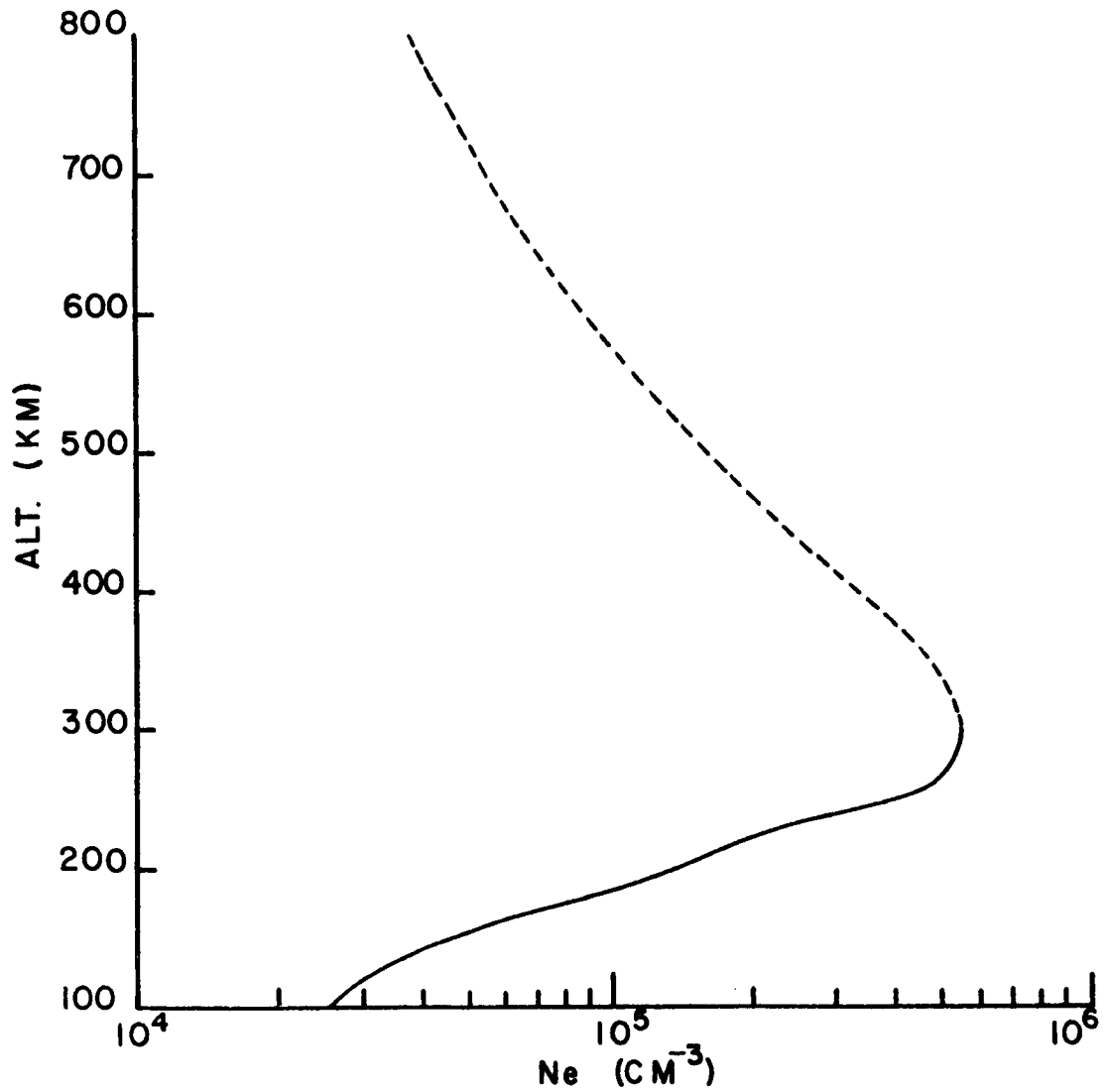
where E is the energy of the photoelectron, n_e is the number density of the ambient electron gas, and x is the path length. The asymptotic form does in fact give satisfactory accuracy down to energies of one electron volt, and its use down to thermal energies does not lead to a very large error (Geisler and Bowhill, 1965).

b. Electron Density Profile

The electron density profile used is shown in Fig. 9. Up to 300 Km the profile is based on the ionograms obtained at Port Stanley (51.7° S), and is extrapolated to the higher altitudes using data obtained by the Alouette I satellite.

c. Results of Calculations

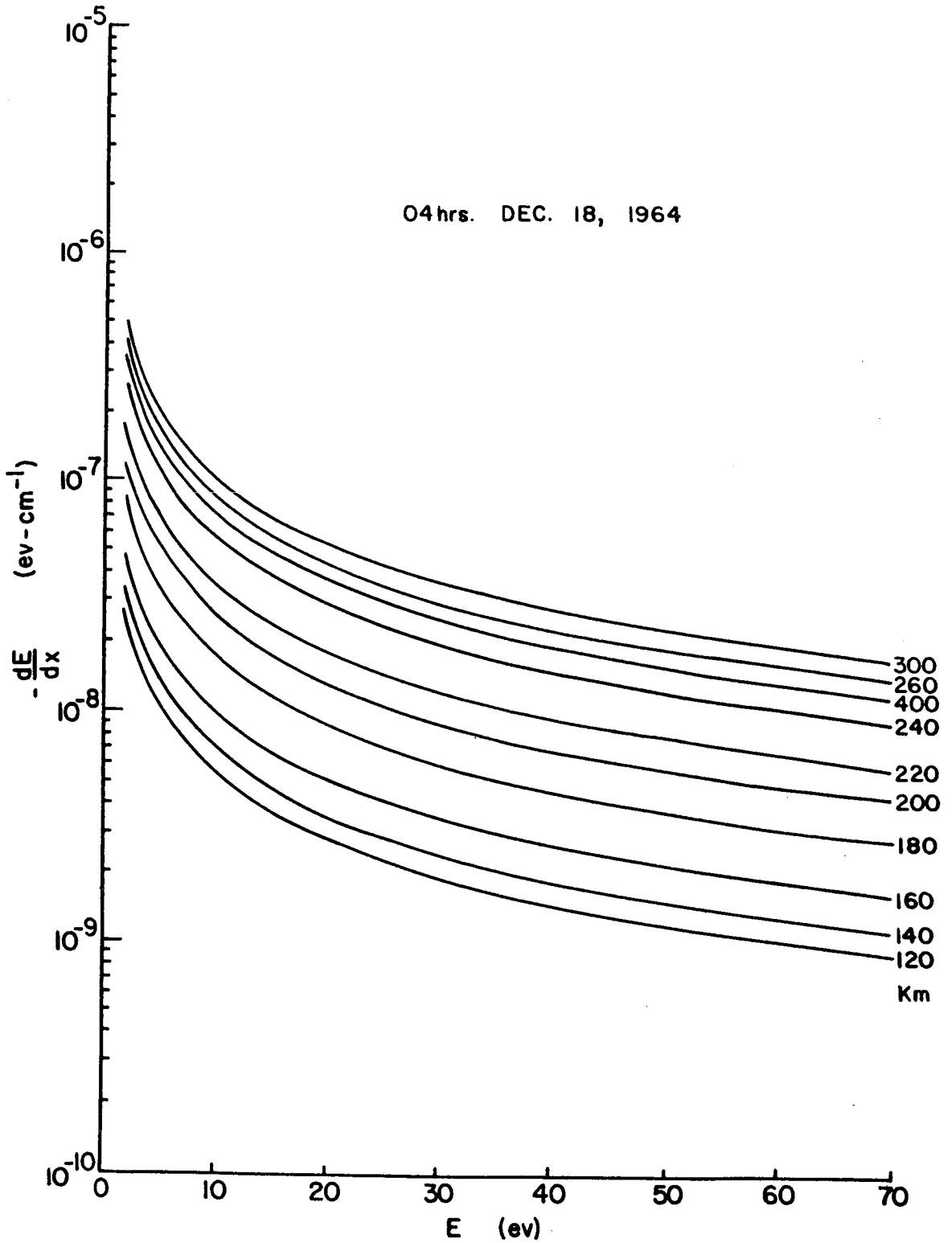
Fig. 10 shows the calculated rates of energy loss of a photoelectron through elastic collisions with the ambient electrons for the altitude range from 120 to 400 Km.



ELECTRON DENSITY IN CONJUGATE
REGION. 04 HRS., DEC. 18, 1964

FIGURE 9

04 hrs. DEC. 18, 1964



RATES OF ENERGY LOSS OF A PHOTOELECTRON TO AMBIENT ELECTRONS IN CONJUGATE REGION

FIGURE 10

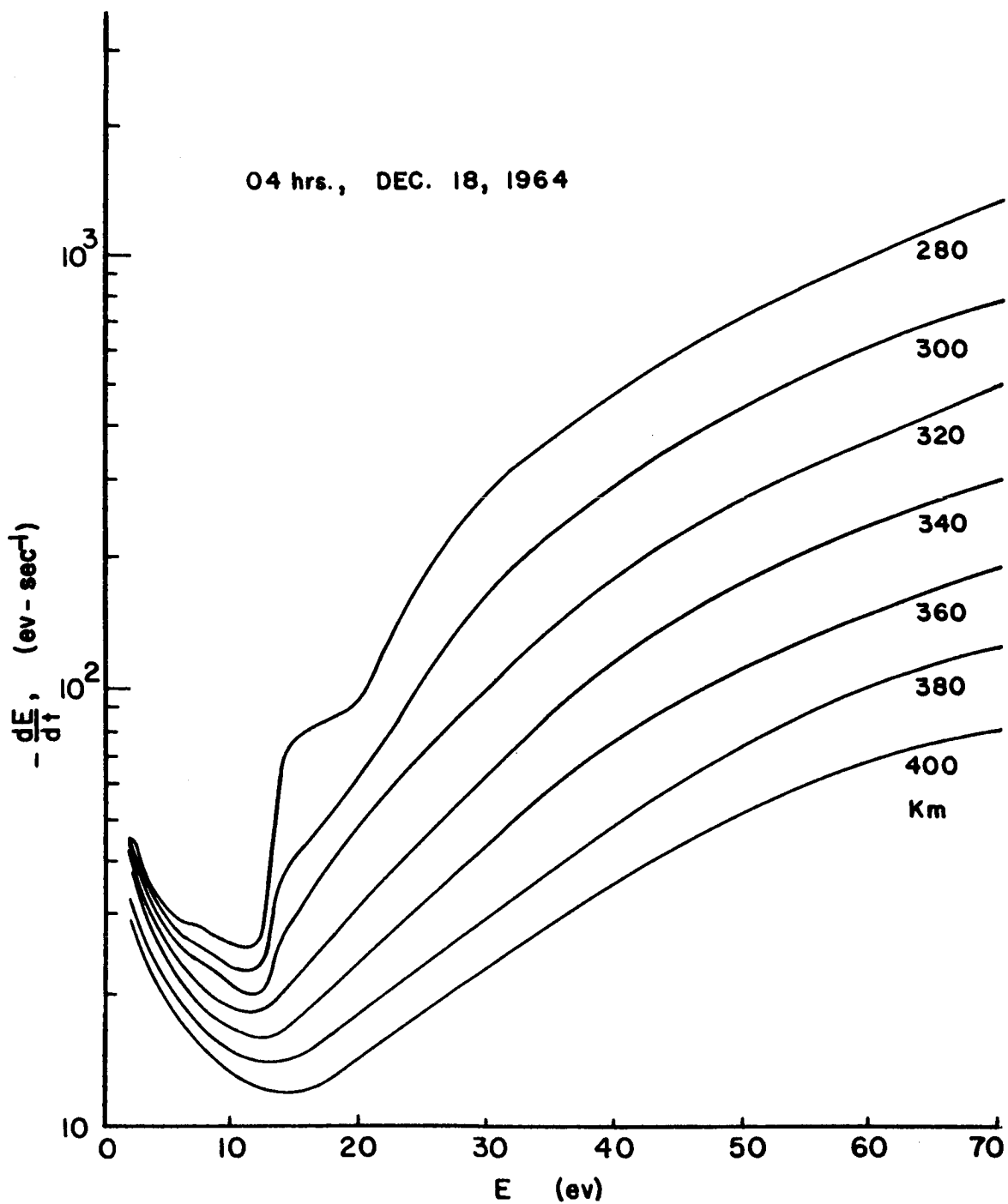
3.4 Total Time Rates of Energy Loss

The time rate of energy loss is related to the spatial rate of energy loss by the following equation:

$$\frac{dE}{dt} = \frac{dE}{dx} \frac{dx}{dt} = \frac{dE}{dx} V = \frac{dE}{dx} \left(\frac{2E}{m_e} \right)^{\frac{1}{2}}, \quad (3.4.1)$$

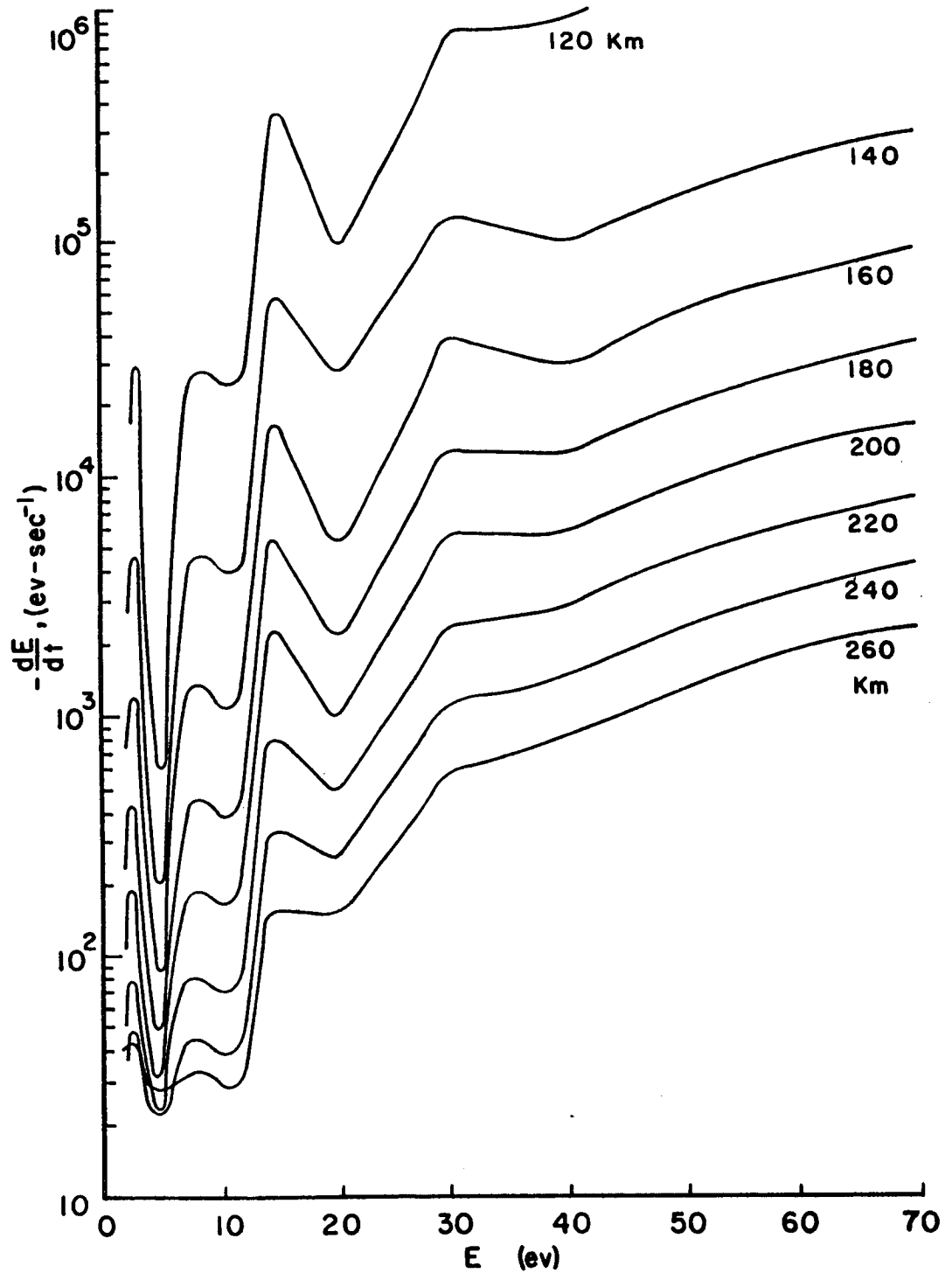
where V is the velocity, E is the energy, and m_e is the mass of the photoelectron. Shown in Fig. 11 are the total time rates of energy loss of a photoelectron due to both elastic collisions with ambient electrons and inelastic collisions with neutral particles.

The production rates of photoelectrons calculated in Section 2 and the loss rates of photoelectrons computed in this section will be used in the calculations of the number densities of photoelectrons as a function of altitude and energy to be discussed in Section 4.



TOTAL TIME RATES OF ENERGY LOSS OF A PHOTOELECTRON TO NEUTRAL PARTICLES AND AMBIENT ELECTRONS IN CONJUGATE REGION

FIGURE II (a)



TOTAL TIME RATES OF ENERGY LOSS OF A PHOTOELECTRON TO NEUTRAL PARTICLES AND AMBIENT ELECTRONS IN CONJUGATE REGION

FIGURE II (b)

4. NUMBER DENSITY OF PHOTOELECTRONS

4.1 Probability of Escape of Photoelectrons Without Further Collision

One of the possible ways to calculate the escaping photoelectron flux at the top of the ionosphere in the sunlit conjugate region of Arecibo is as follows:

Consider a beam of electrons of homogeneous velocity passing through a gas containing n stationary or low energy target particles per cm^3 . Of those electrons that penetrate to a depth x in the gas without experiencing scattering, a fraction equal to $n\sigma dx$ will be scattered in passing from x to $x+dx$. This quantity is also equal to the probability that a given electron that reaches a depth x without scattering will then suffer scattering between x and $x+dx$. Regarding any such impact as removing an electron from the beam, the amount of beam current strength lost in traversing a distance dx from a point p which is at a distance x from o will be given by

$$di = - i(x) n\sigma dx \quad (4.1.1)$$

where $i(x)$ is the unscattered current strength at point p . On integration we have

$$i(x) = i_0 e^{-n\sigma x} \quad (4.1.2)$$

where i_0 represents the initial current strength in electrons per cm^2 per second at $x = 0$. The quantity σ is the total collision cross section of the gas atoms

or molecules for electrons of beam velocity, since the loss from the beam is defined as occurring whenever an electron is deviated from its path or loses energy or both.

If the neutral particle density n is a function of distance, the current density can be written as:

$$i(x) = i_0 e^{-\int_0^x n \sigma dx'} \quad (4.1.3)$$

If there are j constituents of neutral gas then

$$i(x) = i_0 e^{-\int_0^x \sum_j n_j \sigma_j dx'} \quad (4.1.4)$$

To describe the motions of unscattered photoelectrons, it is necessary to introduce two distances, s and x . The length s is a measure of the distance between two points measured along a geomagnetic field line. The length x is, in terms of the same points, measured along the spiral trajectory of a photoelectron. Since the photoelectron follows a helical path, the distance x can be greater than the distance s depending on the pitch angle of the photoelectron. Based on the above considerations, we can write

$$\cos \theta_p = \frac{ds}{dx} \quad (4.1.5)$$

$$\text{Hence, } i(s) = i_0 e^{-\frac{1}{\cos \theta_p} \int_0^s \sum_j n_j \sigma_j ds'} \quad (4.1.6)$$

where θ_p is the pitch angle of the photoelectron. Considering the vertical direction

$$i(z) = i_0 e^{-\frac{\sigma}{\cos \theta_p \sin I} \int_0^z n(z') dz'} \quad (4.1.7)$$

where σ is the average total collision cross section, since the total collision cross section of O, O₂, and N₂ are not much different for the energy range concerned (see Fig. 12). I is the magnetic dip angle. Assuming a constant scale height H of the atmosphere, the escaping photoelectron flux with a pitch angle θ_p is therefore

$$i(\infty) = i_0 e^{-\frac{\sigma n H}{\cos \theta_p \sin I}} = i_0 e^{-\frac{H}{\lambda \cos \theta_p \sin I}} \quad (4.1.8)$$

since $\int_0^\infty n(z') dz' = nH$.

The probability of escape of a photoelectron, or the fraction of photoelectrons that can escape, is equal to

$$p_e = \frac{i(\infty)}{i_0} = e^{-\frac{H}{\lambda \cos \theta_p \sin I}} \quad (4.1.9)$$

where λ is the average total mean free path of the photoelectron.

Next let us assume that the velocities of photoelectrons are isotropic about the geomagnetic field line. From the geometry of Fig. 13, the volume of the spherical sector is equal to

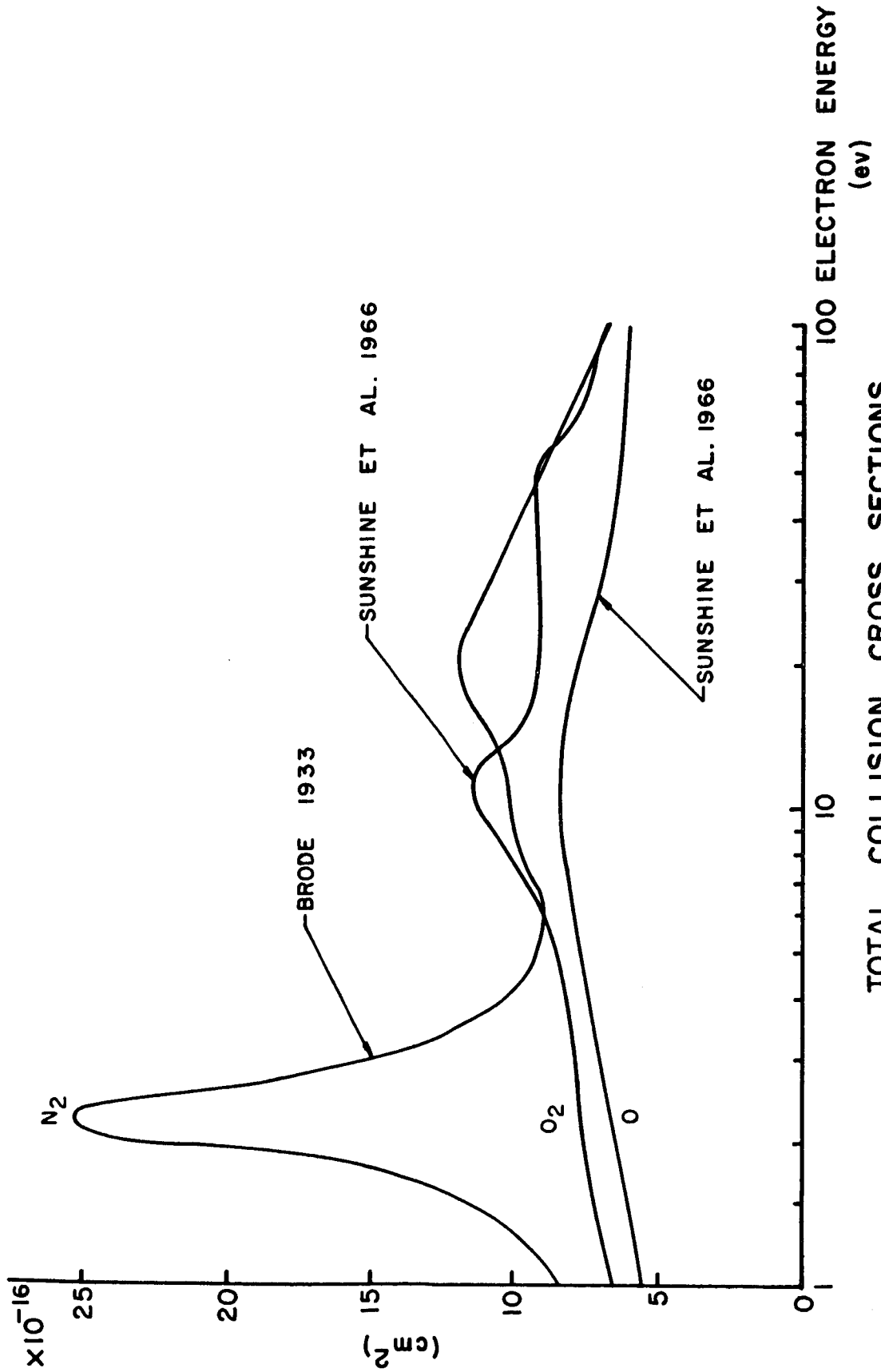
$$d\Omega = \frac{1}{2} (2 \pi r \sin \theta_p) (r d\theta_p) (r) \quad (4.1.10)$$

$$d\Omega = C' \sin \theta_p \quad (4.1.11)$$

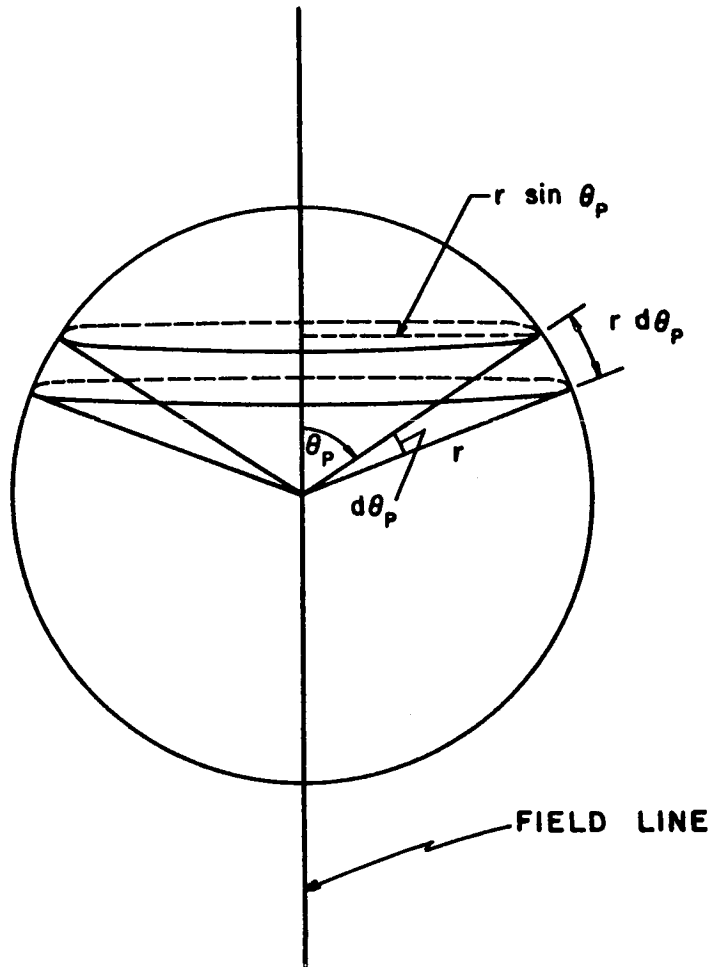
Suppose that the photoelectrons are distributed uniformly, then the number of photoelectrons contained in the spherical sector is proportional to the volume of the spherical sector, i.e.

$$n_p(\theta_p) = C'' \sin \theta_p. \quad (4.1.12)$$

The photoelectron flux in the direction of the field



TOTAL COLLISION CROSS SECTIONS
FIGURE 12



ANGULAR DISTRIBUTION OF PHOTOELECTRONS

FIGURE 13

line is given by

$$\phi(\theta_p) = n_p(\theta_p) V \cos \theta_p \quad (4.1.13)$$

where $n_p(\theta_p)$ is the number density of photoelectrons in the direction θ_p , and V is the velocity of the photoelectrons. Combining Equations (4.1.12) and (4.1.13) gives

$$\phi(\theta_p) = C'' \sin \theta_p V \cos \theta_p = C'' V \sin \theta_p \cos \theta_p \quad (4.1.14)$$

The total photoelectron flux in the direction of the field line is

$$\phi = \sum_{\theta_p=0}^{90^\circ} \phi(\theta_p) = \sum_{\theta_p} C'' V \sin \theta_p \cos \theta_p \quad (4.1.15)$$

and the fractional flux, $\eta(\theta_p)$, is given by

$$\eta(\theta_p) = \frac{\phi(\theta_p)}{\phi} = \frac{\sin \theta_p \cos \theta_p}{\sum_{\theta_p} \sin \theta_p \cos \theta_p} \quad (4.1.16)$$

4.2 Continuity Equation for the Photoelectron Number Density

The continuity equation

$$\frac{\partial n_p}{\partial t} = q - L - \text{div}(n_p V_z) \quad (4.2.1)$$

can be written for the photoelectrons produced in the conjugate region. The solution of this equation is extremely complicated because in the upper F region the energy loss of a photoelectron through elastic collisions with the ambient electrons is comparable with that through inelastic collisions with the neutral particles while

the transport of a photoelectron is considerably affected by elastic collisions with the neutrals. At the higher energy levels a photoelectron may lose several electron volts in a single inelastic collision with the neutrals and the angle between the photoelectron velocity and the local magnetic field must be considered.

In the approach adopted here, the analysis starts with the assumption of steady state conditions and as an initial approximation neglects the transport term. Based on this approximation, it is possible to calculate the photoelectron number densities as a function of altitude and energy in a manner somewhat similar to that employed by Hoegy et al. (1965). In this analysis, the altitude region has been broken up into a number of height increments and the energy spectrum of photoelectrons has been broken up into one electron volt increments.

Assuming steady state and neglecting the transport term, the continuity equation becomes

$$q = L \quad (4.2.2)$$

If γ is the highest energy of photoelectrons produced by solar radiation, then the production term is simply

$$q_{s\gamma} = L_{1\gamma} + L_{e\gamma} \quad (4.2.3)$$

where $q_{s\gamma}$ is the production rate of photoelectrons due to solar radiation. $L_{1\gamma}$ is the loss rate of photoelectrons due to local energy loss to both neutral particles and ambient electrons. From Equation (3.4.1)

$$L_{1\gamma} = n_{p\gamma} \left. \frac{dE}{dt} \right|_{\gamma} \quad (4.2.4)$$

$L_{e\gamma}$ is the loss rate of photoelectrons due to escape, and

$$L_{e\gamma} = n_{p\gamma} \frac{v}{\lambda} \sum_{\theta_p=0^\circ}^{90^\circ} \frac{1}{2} \eta(\theta_p) e^{-\frac{H}{\lambda \cos \theta_p \sin I}} \quad (4.2.5)$$

$$L_{e\gamma} = n_{p\gamma} K_{\gamma} \quad (4.2.6)$$

where

$$K_{\gamma} = \frac{v}{2\lambda} \sum_{\theta_p=0^\circ}^{90^\circ} \eta(\theta_p) e^{-\frac{H}{\lambda \cos \theta_p \sin I}} \quad (4.2.7)$$

Hence,

$$q_{s\gamma} = n_{p\gamma} \left(\left. \frac{dE}{dt} \right|_{\gamma} + K_{\gamma} \right) \quad (4.2.8)$$

$$n_{p\gamma} = \frac{q_{s\gamma}}{\left. \frac{dE}{dt} \right|_{\gamma} + K_{\gamma}} \quad (4.2.9)$$

$$L_{1\gamma} = n_{p\gamma} \left. \frac{dE}{dt} \right|_{\gamma} \quad (4.2.10)$$

Substituting Eq. (4.2.9) into Eq. (4.2.10) we have

$$L_{1\gamma} = q_{s\gamma} \left\{ \frac{\left. \frac{dE}{dt} \right|_{\gamma}}{\left. \frac{dE}{dt} \right|_{\gamma} + K_{\gamma}} \right\} = q_{s\gamma} \left\{ \frac{1}{1 + \frac{K_{\gamma}}{\left. \frac{dE}{dt} \right|_{\gamma}}} \right\} \quad (4.2.11)$$

$$L_{1\gamma} = q_{S\gamma} P_{\gamma} \quad (4.2.12)$$

where

$$P_{\gamma} = \frac{1}{1 + \frac{K_{\gamma}}{\left. \frac{dE}{dt} \right|_{\gamma}}} \quad (4.2.13)$$

P_{γ} is the probability that a photoelectron will lose energy locally in going from γ ev. to $(\gamma-1)$ ev.

For the next lower energy level we can write

$$q_{(\gamma-1)} = L_{(\gamma-1)} \quad (4.2.14)$$

$$q_{(\gamma-1)} = q_{S(\gamma-1)} + L_{1\gamma} \quad (4.2.15)$$

The first term on the right is the production term due to solar radiation, and the second term is due to the energy-degradation of the next higher energy level.

Combining Eqs. (4.2.14) and (4.2.15) we have

$$q_{S(\gamma-1)} + I_{1\gamma} = L_{1(\gamma-1)} + L_{e(\gamma-1)} \quad (4.2.16)$$

or

$$q_{S(\gamma-1)} + q_{S\gamma} P_{\gamma} = n_{p(\gamma-1)} \left\{ \left. \frac{dE}{dt} \right|_{(\gamma-1)} + K_{(\gamma-1)} \right\} \quad (4.2.17)$$

from which we can write

$$n_{p(\gamma-1)} = \frac{q_{S(\gamma-1)} + q_{S\gamma} P_{\gamma}}{\left. \frac{dE}{dt} \right|_{(\gamma-1)} + K_{(\gamma-1)}} \quad (4.2.18)$$

$$L_{1(\gamma-1)} = n_{p(\gamma-1)} \left. \frac{dE}{dt} \right|_{(\gamma-1)} = \left\{ q_{s(\gamma-1)} + q_{s\gamma} P_{\gamma} \right\} \left\{ \frac{\frac{dE}{dt} (\gamma-1)}{\frac{dE}{dt} (\gamma-1) + K(\gamma-1)} \right\} \quad (4.2.19)$$

$$= \left\{ q_{s(\gamma-1)} + q_{s\gamma} P_{\gamma} \right\} P_{(\gamma-1)}$$

$$= q_{s\gamma} P_{\gamma} P_{(\gamma-1)} + q_{s(\gamma-1)} P_{(\gamma-1)} \quad (4.2.20)$$

In general then

$$L_{1n} = \sum_{m=n}^{\gamma} q_{sm} \prod_{i=n}^m P_i \quad (4.2.21)$$

But
$$L_{1n} = n_{pn} \left. \frac{dE}{dt} \right|_n \quad (4.2.22)$$

from which we can determine the number density of photoelectrons

$$n_{pn} = \frac{\sum_{m=n}^{\gamma} q_{sm} \prod_{i=n}^m P_i}{\left. \frac{dE}{dt} \right|_n} \quad (4.2.23)$$

4.3 Height Profiles of Photoelectron Number Density

The calculated height profiles of photoelectron number density are shown in Fig. 14 and 15. From these figures we note the following:

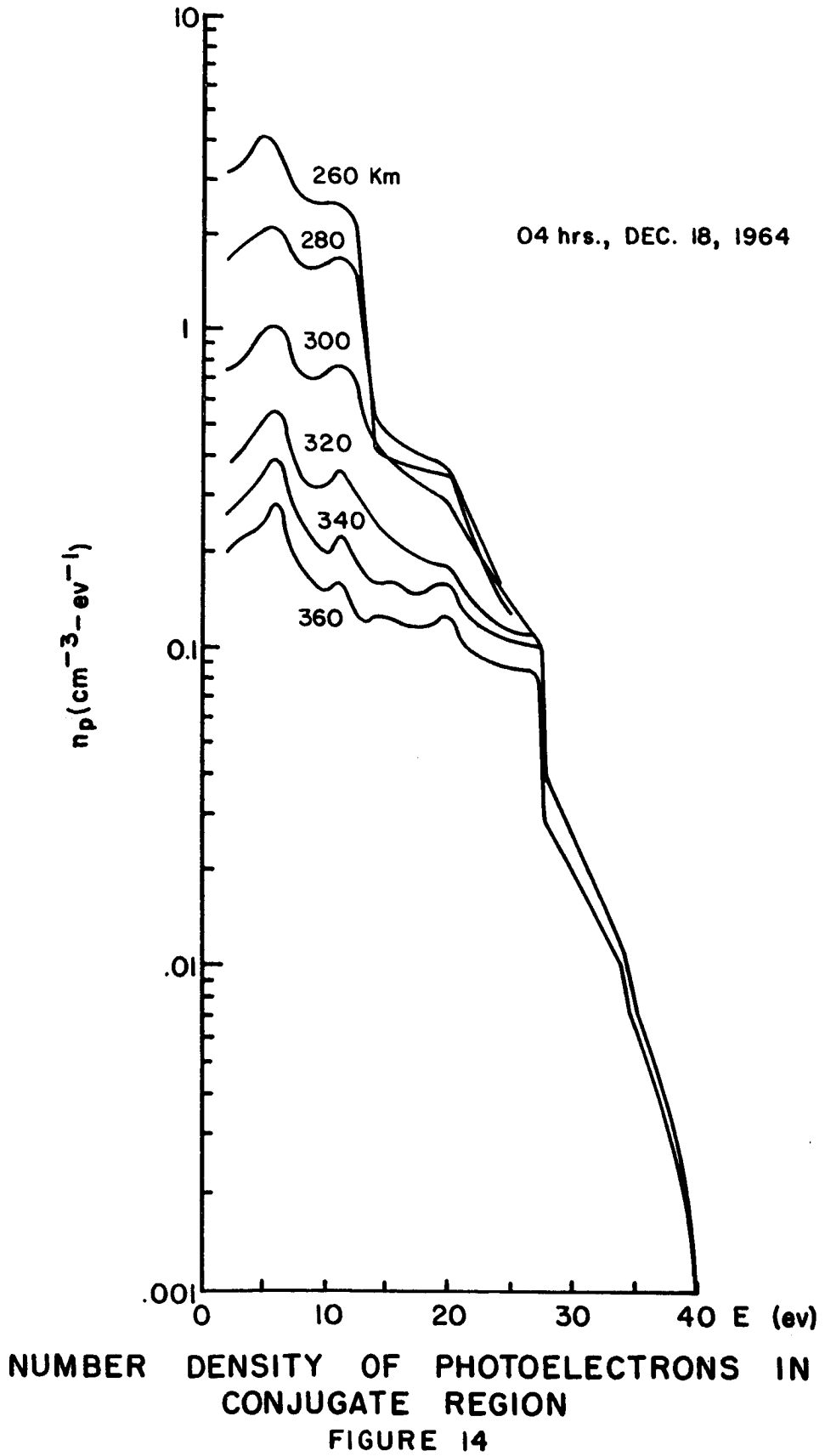
- (a) For electron energies lower than about 13 ev. the gradients of number density of photoelectrons are large below about 300 Km compared to those

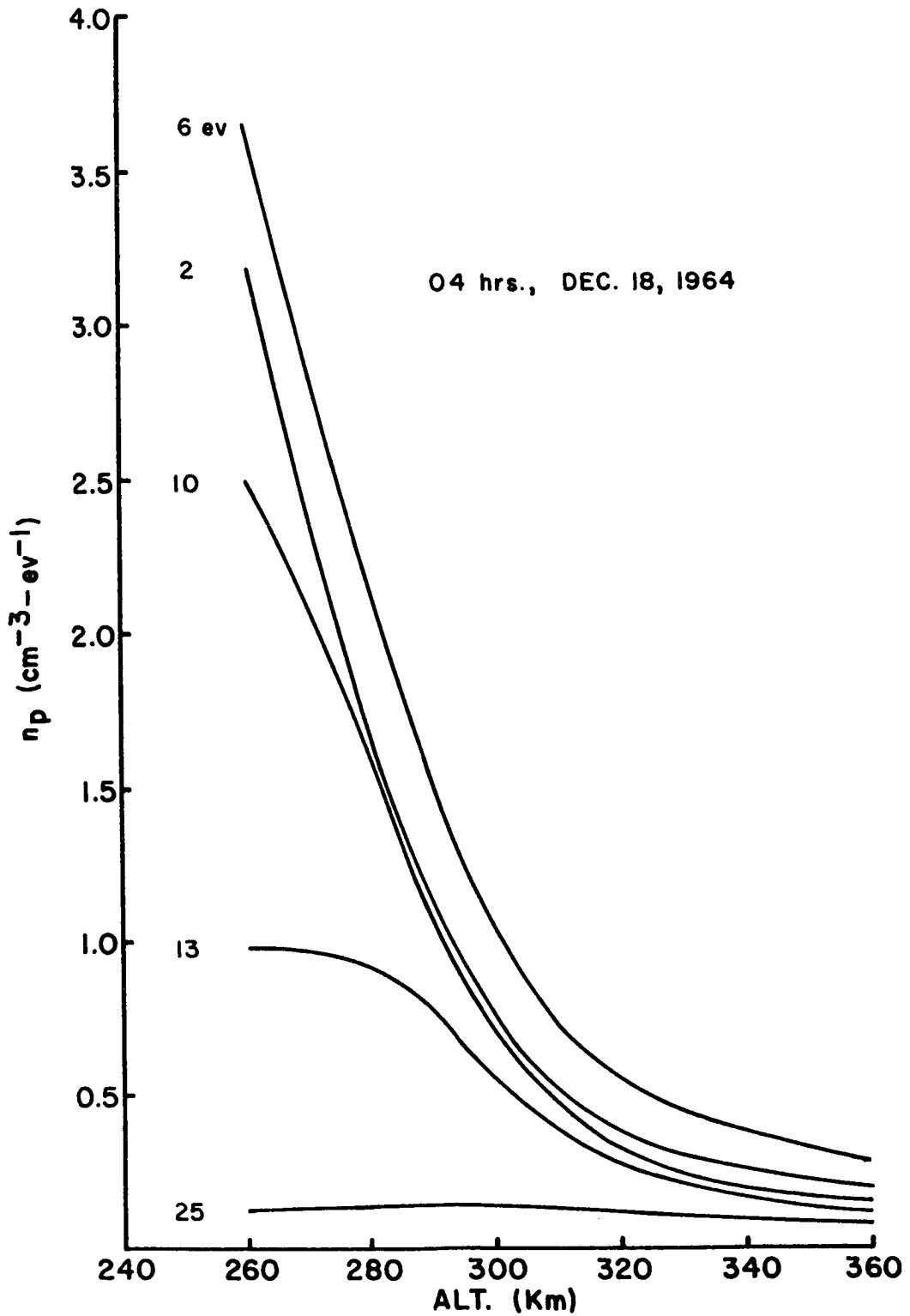
above this altitude. This is because below the altitude of 300 Km. and below the electron energy of 13 ev. the electronic and vibrational excitations of N_2 are the dominant loss processes which change quite rapidly with altitude. Above the 300 Km. level and below 13 ev. the energy-loss to the ambient electrons which varies more slowly with height (the ambient electron density has a peak in the neighborhood of 300 Km.) becomes more important. This behavior has an important effect on the diffusion flux of photoelectrons which will be discussed later.

- (b) Up to about 30 ev. the number density of photoelectrons is generally decreasing with increasing altitude above the 260 Km. level. But the number density of photoelectrons is practically independent of the altitude for energies above 30 ev. and above 260 Km.

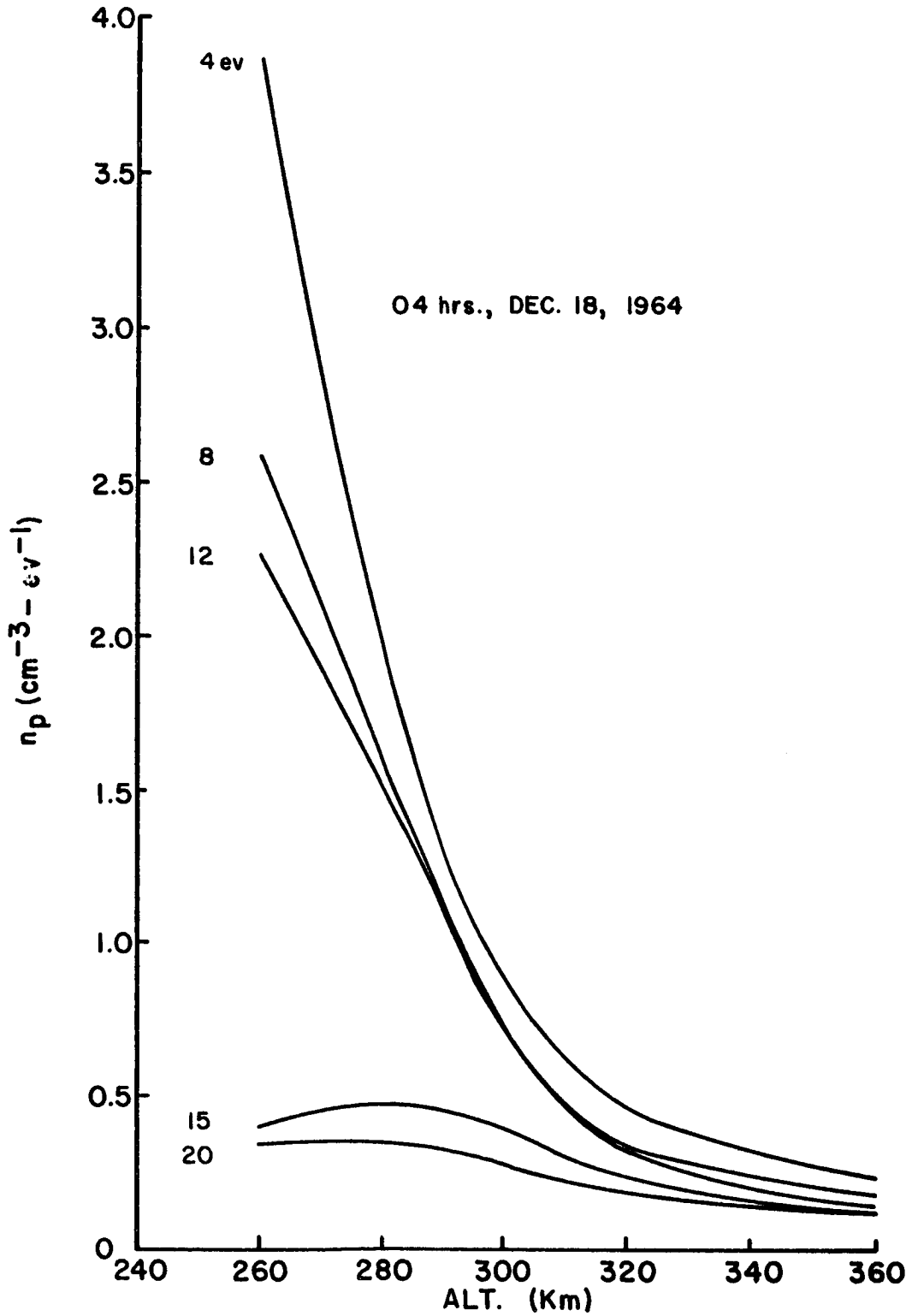
The calculations of the photoelectron number densities have been done neglecting the divergence of the diffusion flux. The range of altitudes over which this approximation is valid will be discussed in Section 5.

Having calculated the number densities of photoelectrons, it is now possible to compute the photoelectron diffusion flux leaving the conjugate region as will be discussed in Section 5.





NUMBER DENSITY OF PHOTOELECTRONS IN
CONJUGATE REGION
FIGURE 15(a)



NUMBER DENSITY OF PHOTOELECTRONS IN
CONJUGATE REGION
FIGURE 15(b)

5. UPWARD-GOING PHOTOELECTRON FLUXES

5.1 Diffusion Flux of Photoelectrons

As has been pointed out in Section 3.1.1, the energetic photoelectron loses only a little energy in an elastic collision with the neutral particles, but the angle of scattering may be quite large and tends to randomize the direction of a photoelectron. Thus, the elastic collisions with neutral particles play an important role in controlling the diffusion flux of photoelectrons in an upward direction.

The diffusion velocity of photoelectrons is given by Nisbet (1967)

$$V_z = - \frac{V\lambda}{6 n_p} \frac{dn_p}{dz} \sin^2 I \quad (5.1.1)$$

where V is the velocity of the photoelectrons, λ is the mean distance to randomize the direction of a photoelectron in elastic collisions with neutral particles, n_p is the number density of photoelectrons in a given energy range, $\frac{dn_p}{dz}$ is the gradient of the number density of photoelectrons in the vertical direction, and I is the magnetic dip angle.

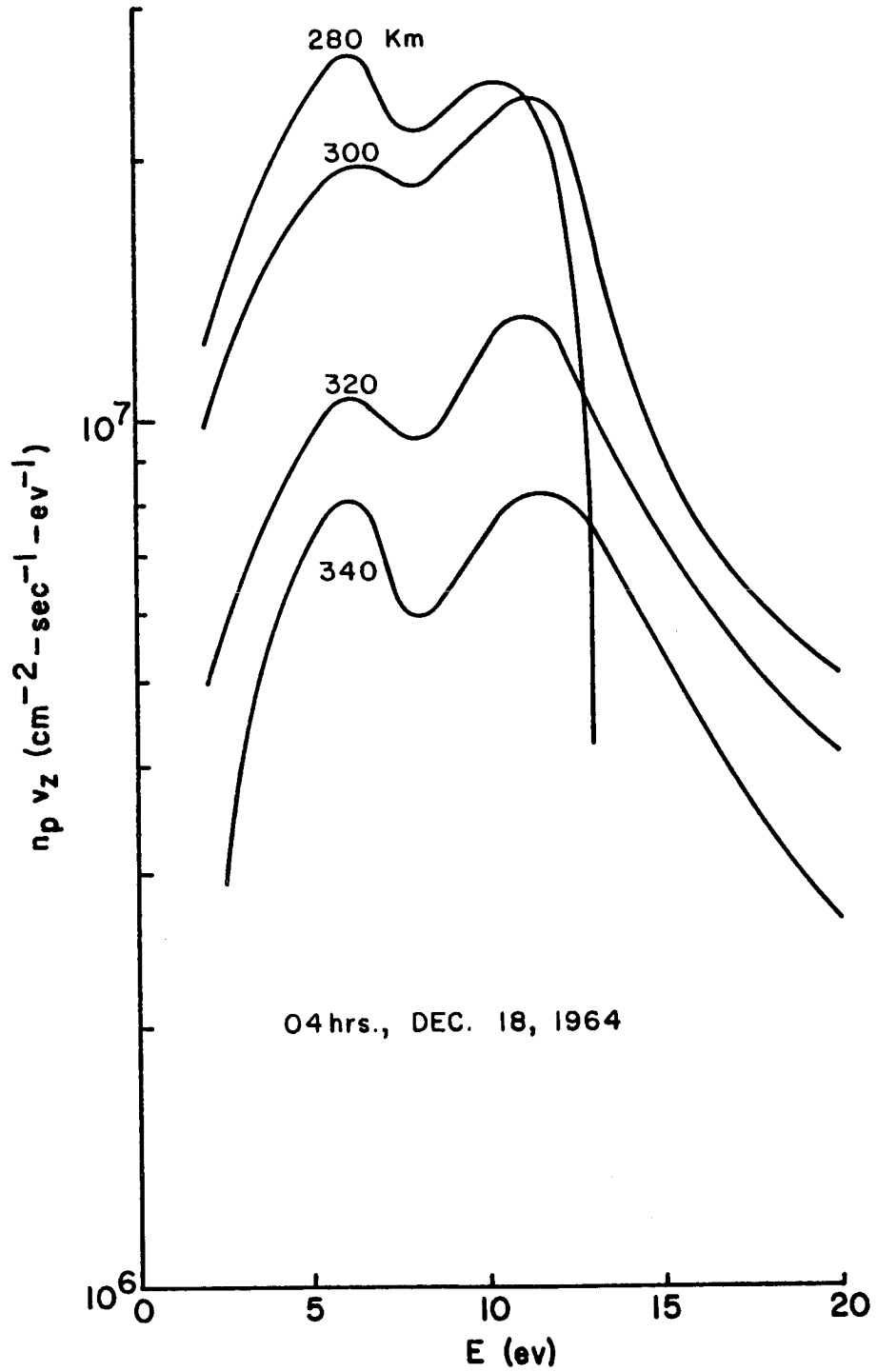
The diffusion flux of photoelectrons in each energy range is

$$\phi_d = n_p V_z \quad (5.1.2)$$

$$\phi_d = - \frac{V\lambda}{6} \frac{dn_p}{dz} \sin^2 I \quad (5.1.3)$$

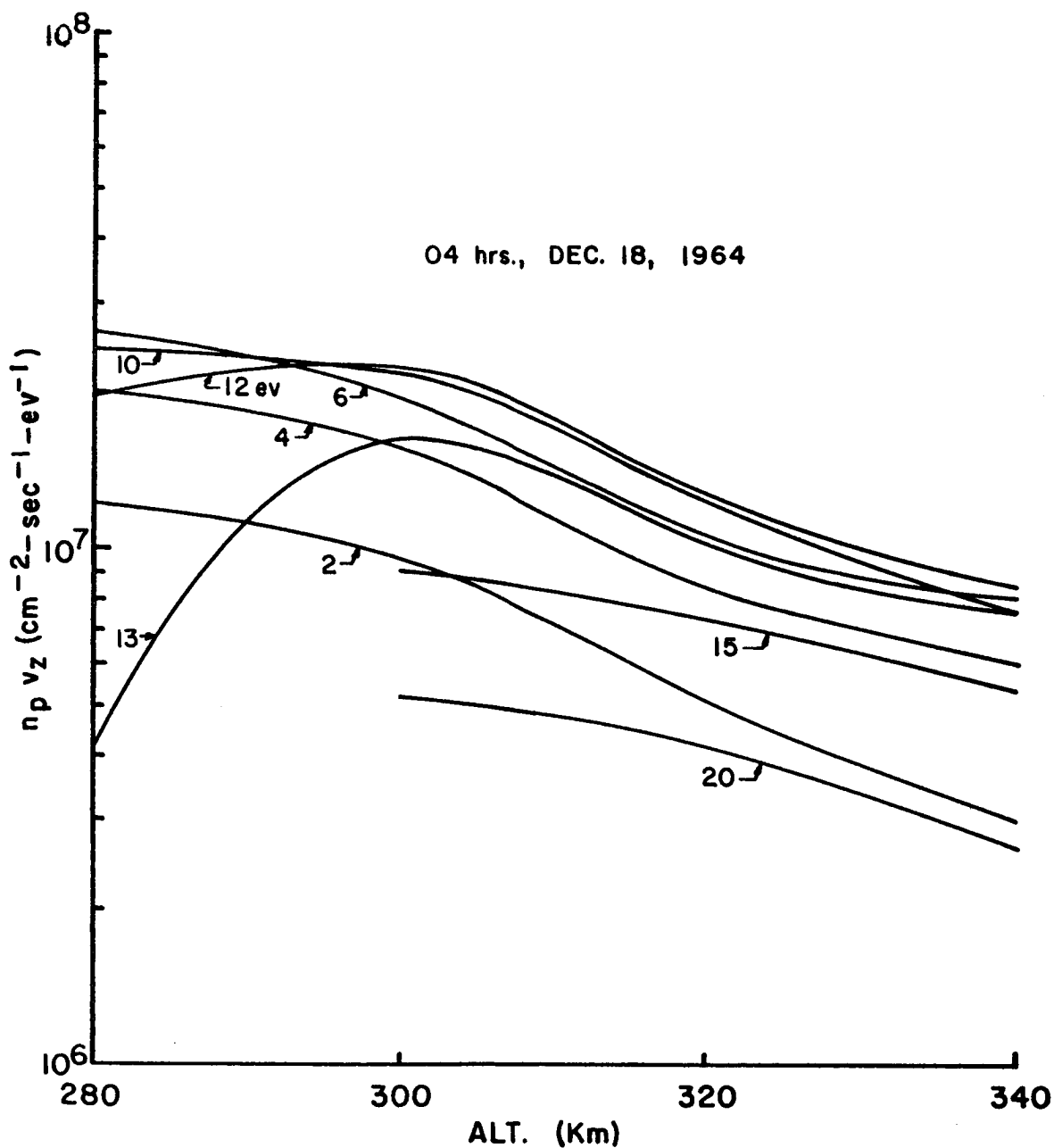
The calculated diffusion fluxes of photoelectrons are shown in Fig. 16 and 17. It is apparent that the diffusion flux of photoelectrons is cut off at about 30 ev. since the number density of photoelectrons is practically independent of the altitude above the 260-Km level and above 30 ev. (see Section 4.3). It can be seen from Fig. 17 that the diffusion fluxes of photoelectrons decrease slowly with increasing height above the 300-Km level. This is because the mean free path of photoelectrons does not increase as rapidly with increasing altitudes as does the gradient of the number density of photoelectrons decrease. As has been explained in Section 4.3, for electron energies lower than about 13 ev. and above about 300 Km. the predominant energy-loss of a photoelectron is that due to ambient electrons which vary rather slowly between 280 and 400 Km. in the model adopted here (see Fig. 9). Hence, the number density of photoelectrons changes slowly, and its gradient drops to a low value in this altitude region and energy range.

The calculated divergence of the diffusion flux of photoelectrons is plotted in Fig. 18 in comparison with the production rates and loss rates of photoelectrons for two electron energy intervals. In general the divergence term is seen to be small compared to the total production term and total loss term in the continuity equation.



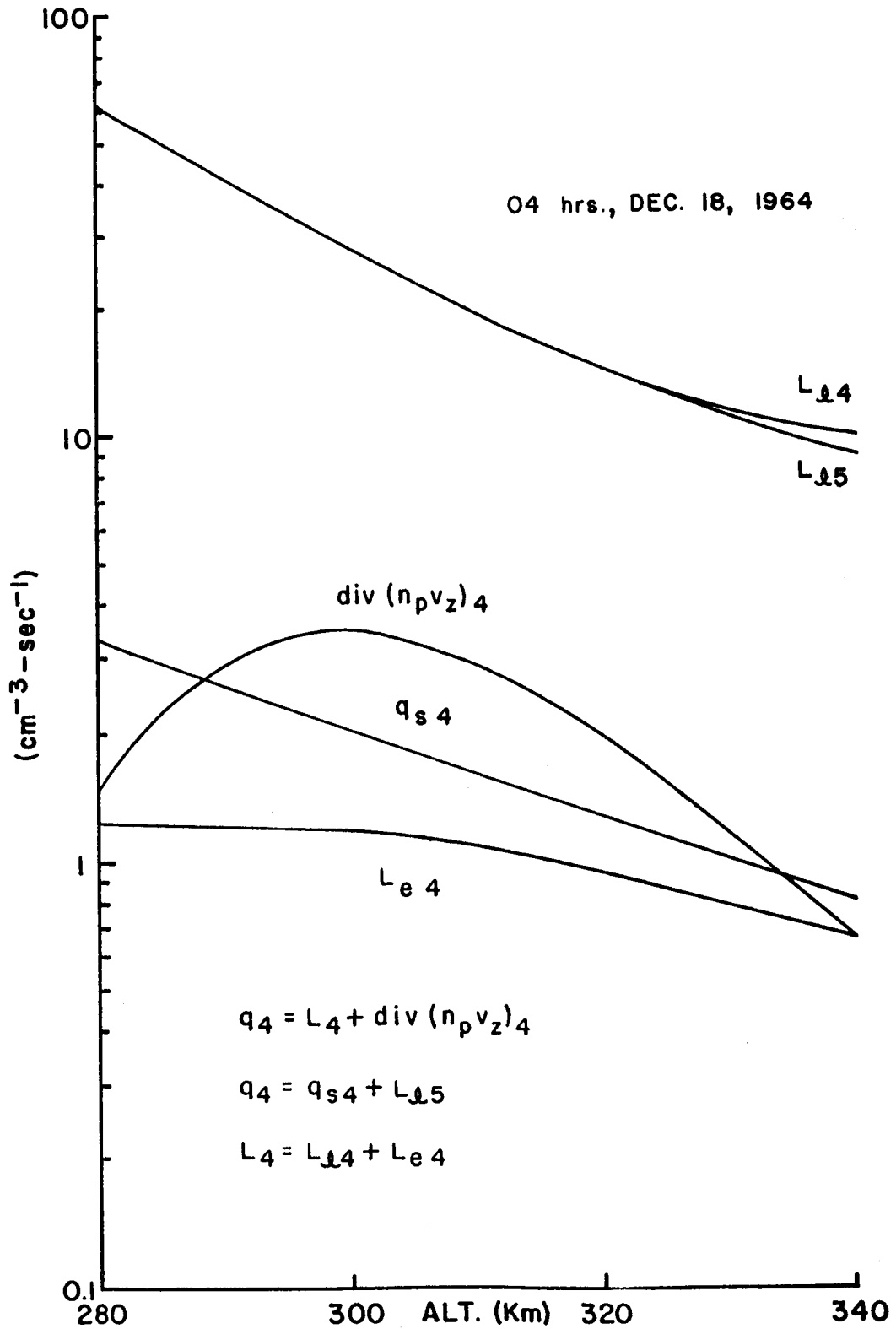
DIFFUSION FLUX OF PHOTOELECTRONS IN
CONJUGATE REGION

FIGURE 16

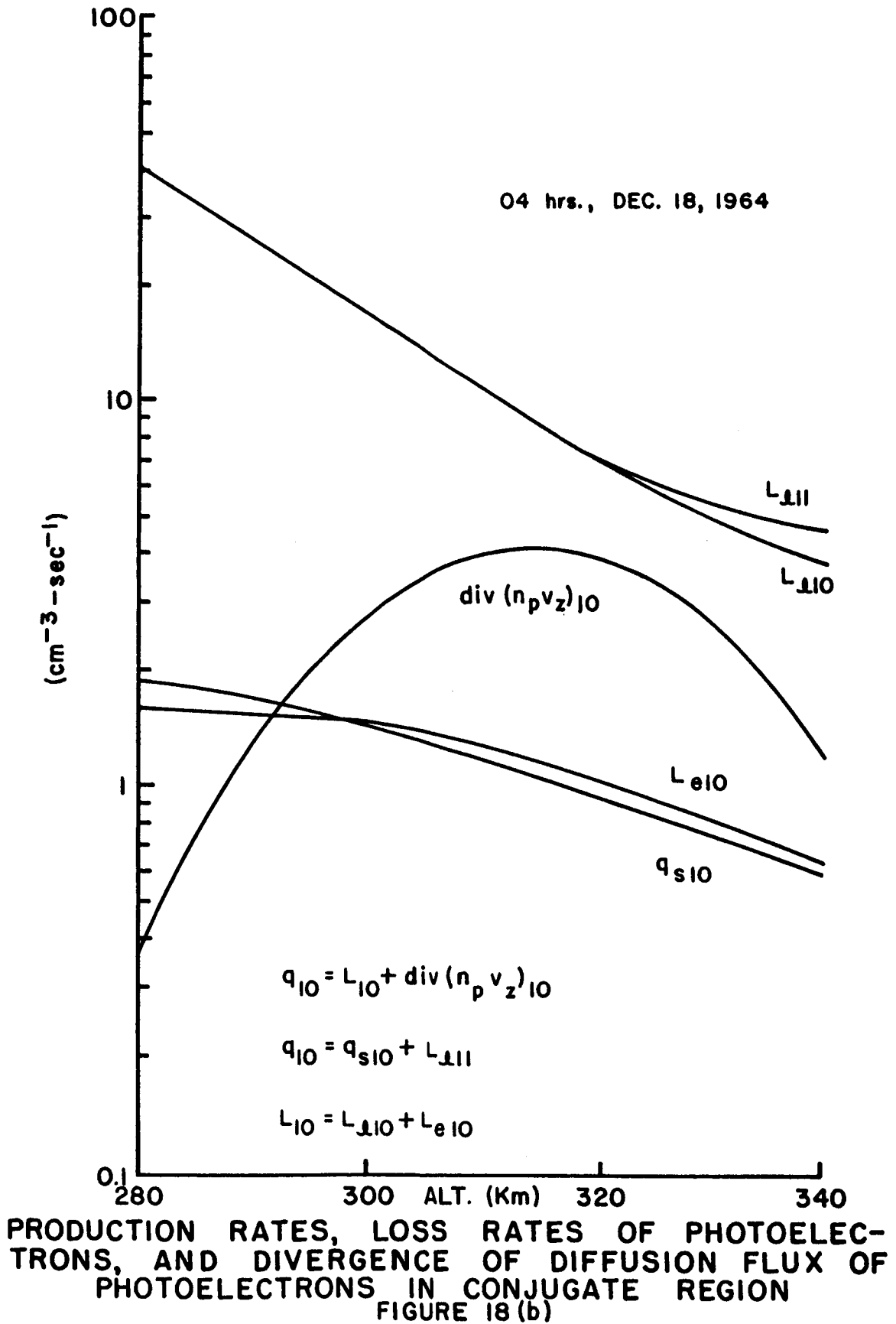


DIFFUSION FLUX OF PHOTOELECTRONS
IN CONJUGATE REGION

FIGURE 17



PRODUCTION RATES, LOSS RATES OF PHOTOELECTRONS, AND DIVERGENCE OF DIFFUSION FLUX OF PHOTOELECTRONS IN CONJUGATE REGION
FIGURE 18 (a)



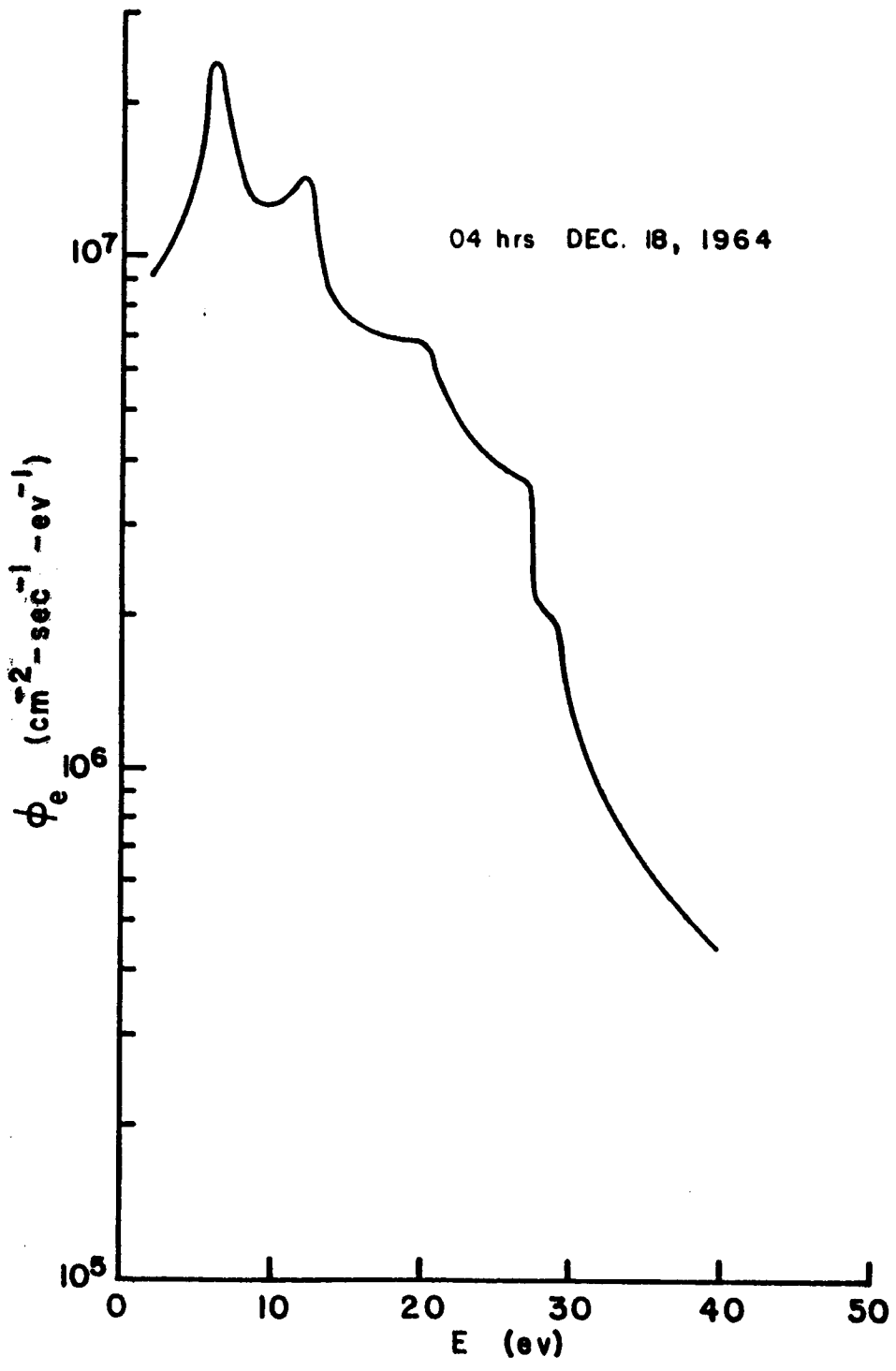
5.2 Escaping Flux of Photoelectrons

Equation (4.2.5) gives the number of photoelectrons escaping per cm^3 per second. The escaping flux of photoelectrons for energy range γ is then given by

$$\phi_{e\gamma} = \int_0^{\infty} L_{e\gamma} dz \quad (5.2.1)$$

The calculated energy spectrum of escape flux of photoelectrons is shown in Fig. 19. The escape flux is comparable in magnitude with the diffusion flux between 280 and 320 Km. (See Figs. 16 and 19).

Having calculated the upward-going diffusion flux and escape flux of photoelectrons from the conjugate region, the next relevant calculations are the determinations of the heat deposited in the protonosphere due to this photoelectron flux. This will be considered in Section 6.



ESCAPE FLUX OF PHOTOELECTRONS
IN CONJUGATE REGION

FIGURE 19

6. ENERGY DEPOSITED IN THE PROTONOSPHERE AND THE DOWNWARD HEAT FLUX

6.1 Basic Equation

The conjugate point photoelectrons gradually lose their energy to the ambient electrons along the magnetic field line through elastic collisions and some of them become thermal before reaching Arecibo. Thus, the phototelectron flux is attenuated gradually along the field line. The photoelectron energy flux along the field line is given by

$$H_s = \sum_{E_o} \sum_{\theta_p} E_s(E_o, \theta_p) \phi(E_o, \theta_p) \quad (6.1.1)$$

where

$$E_s = \sqrt{E_o^2 - \frac{3.9 \times 10^{-12}}{\cos \theta_p}} \int_0^s n_e ds' \quad (6.1.2)$$

which can be derived from Eq. (3.3.1) or

$$\frac{dE}{ds} = - \frac{1.95 \times 10^{-12} n_e}{E \cos \theta_p} \quad (6.1.3)$$

and ϕ is the total upward-going flux of photoelectrons from the conjugate region which is the sum of the escape flux and diffusion flux at the 300-Km level since the diffusion flux tends to level off above 300-Km.

The heat flux due to the conduction of ambient electrons along the field line is given by

$$\mathcal{H}_s = K_e \frac{dT_e}{dz} \sin I \quad (6.1.4)$$

where K_e is the thermal conductivity of the electron gas along the magnetic field line. Spitzer (1962) has developed an expression for K_e :

$$K_e = 7.7 \times 10^5 T_e^{5/2} \text{ ev/cm-sec-deg.} \quad (6.1.5)$$

6.2 Line Integral of the Electron Density Along the Field Line

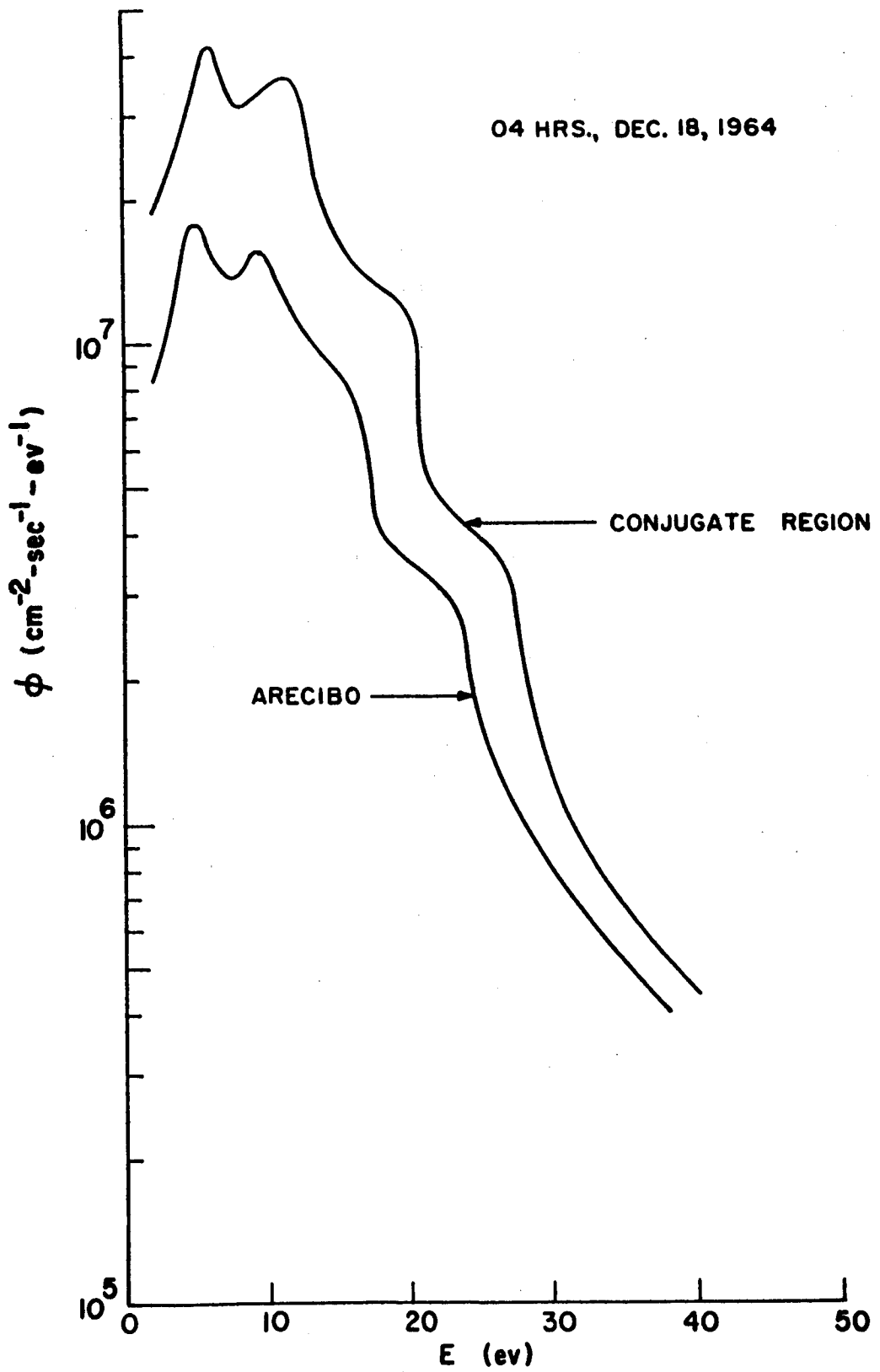
The electron density at the 3000 Km. level above Jicamarca, Peru, measured by Farley in the early morning on February 3, 1965, is about 10^4 cm^{-3} . According to Brace and Reddy (1965), the electron density at the 1000-Km. level, $50^\circ\text{S}-50^\circ\text{N}$ mag. measured by Explorer XXII at night (0000-0330 hrs.) on November-December 1964 is between 10^4 and about $2.5 \times 10^4 \text{ cm}^{-3}$. Based on these measurements it seems reasonable to assume the line integral of the electron density above 1000 Km. to be 10^{13} cm^{-2} .

6.3 Results of Calculations

Fig. 20 shows the photoelectron fluxes at both ends of the field line. The photoelectron flux of Arecibo is about $2 \times 10^8 \text{ electrons-cm}^{-2}\text{-sec}^{-1}$ which is approximately 40% of that leaving the conjugate region.

Fig. 21 shows the variation of the photoelectron energy flux along the field line above 300 Km. It can be seen that the energy deposited along the field line above an altitude of 1000 Km. is about $1 \times 10^9 \text{ ev-cm}^{-2}\text{-sec}^{-1}$. This heat is conducted downwards at both ends of the field line. The heat flux conducted downwards from the 1000-Km. level at the Arecibo end of the field line is compared with values calculated from the electron temperature gradients measured at Arecibo in Fig. 22. It can be seen that the extrapolated measured heat flux agrees quite well with the theoretical heat flux conducted downwards from the 1000-Km. level. Difficulties in interpretation of the measurement of temperature when the relative densities of atomic oxygen, helium and hydrogen ions are varying make such heat conduction measurements uncertain above 450 Km. for these observations.

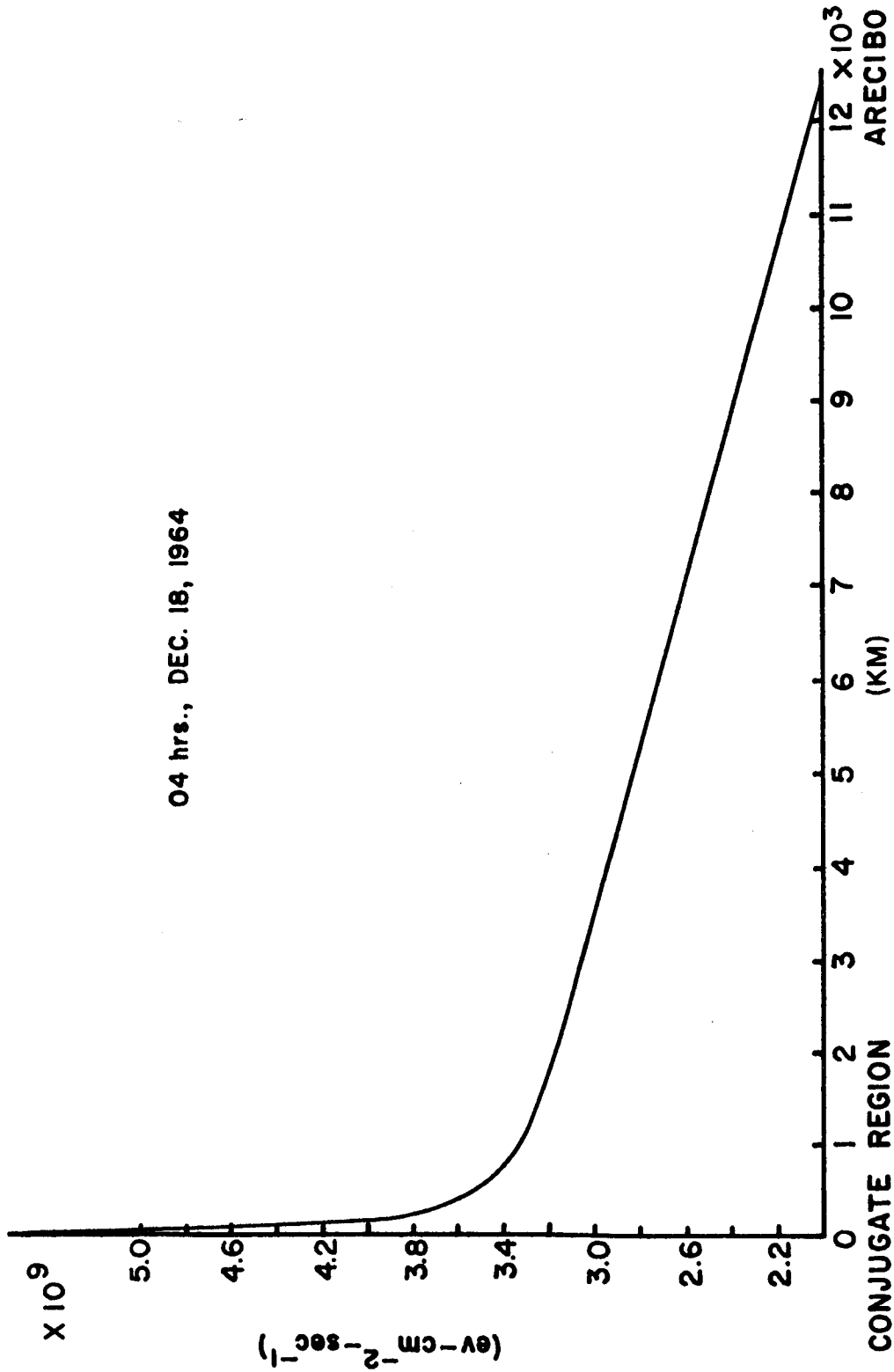
The next step is to calculate the heat input to the ambient electrons and the energy required to excite the oxygen red line in the dark ionosphere above Arecibo during the predawn period due to the incoming photoelectrons from the conjugate region. This will be discussed in Sections 7 and 8.



PHOTOELECTRON FLUX ABOVE 300 KM

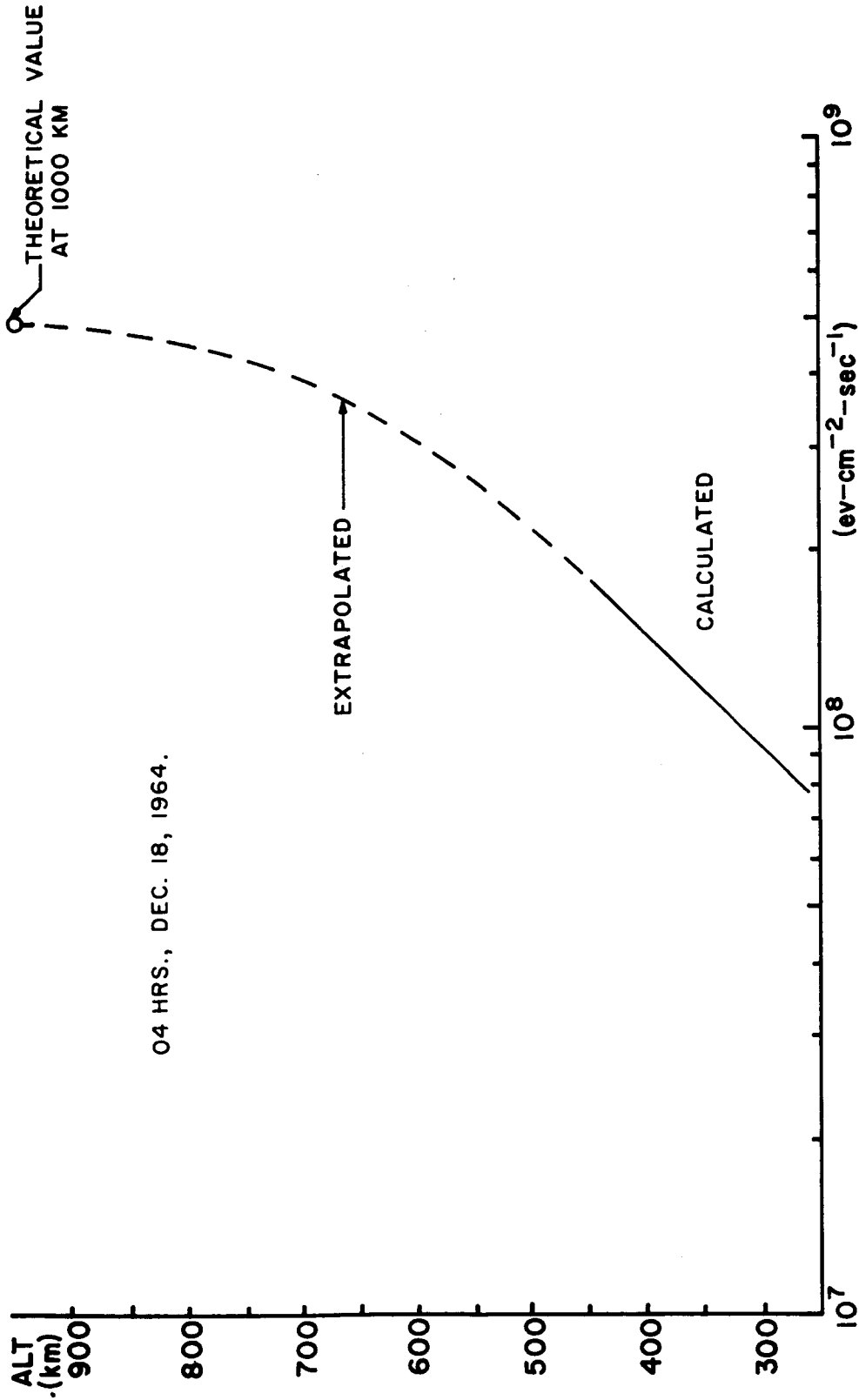
FIGURE 20

04 hrs., DEC. 18, 1964



PHOTOELECTRON ENERGY FLUX ALONG THE FIELD LINE ABOVE 300 KM

FIGURE 21



DOWNWARD HEAT FLUX DUE TO CONDUCTION AT ARECIBO

FIGURE 22

7. HEAT INPUT TO THE AMBIENT ELECTRONS
IN THE DARK IONOSPHERE DUE TO MAGNETIC
CONJUGATE POINT PHOTOELECTRONS

The attenuation of the downward-going photoelectron flux is given by (See Equations (4.1.6) and (4.1.7)).

$$\phi = \phi(z'') = \phi_0 e^{-\frac{1}{\cos\theta_p \sin I} \int_0^{z''} \sum_{j=1} \sigma_j n_j dz'} \quad (7.1)$$

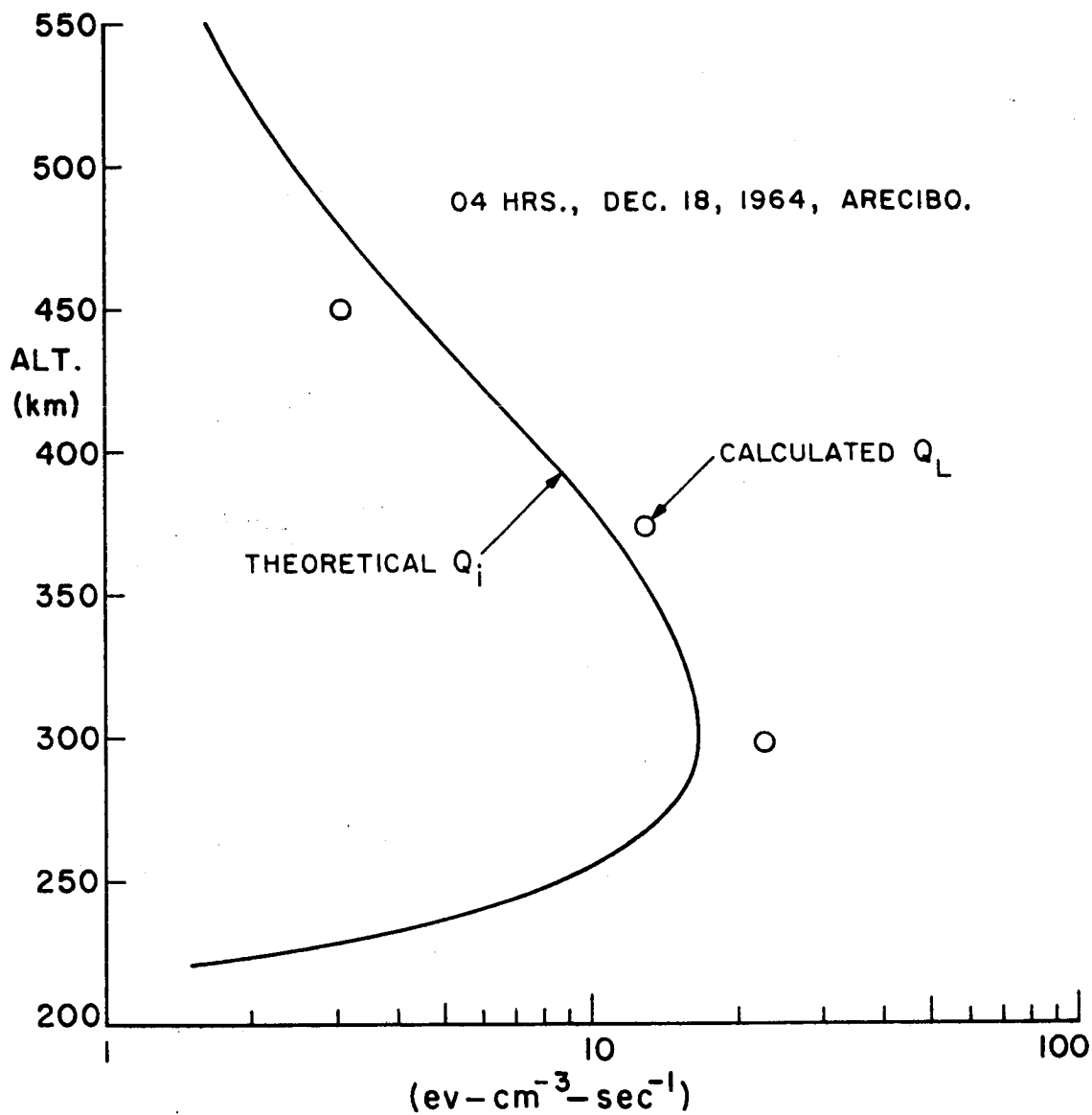
where z' is chosen to be zero at the 300 Km. level, and is positive in the downward direction; ϕ_0 is the incoming photoelectron flux at 300 Km.; n_j is the number density of the j th constituent of the neutrals; σ_j is the collision cross section for electron in the j th constituent of the neutral particles; I is the magnetic dip angle; and θ_p is the pitch angle of the photoelectron.

As the incoming photoelectrons spiral down the field line, they lose their energy through elastic collisions to the ambient electrons in the dark ionosphere above Arecibo. The heat input to the ambient electrons due to the incident photoelectron fluxes is given by

$$Q_i = \frac{dE}{dz} \phi \quad (7.2)$$

$$Q_i = \sum_{E_o} \sum_{\theta_p} \frac{1.95 \times 10^{-12} n_e \phi(E_o, \theta_p)}{\sin I \cos \theta_p E_s(E_o, \theta_p)} \quad (7.3)$$

Figure 23 shows the height profile of this theoretical heat input in comparison with the measured total energy losses of ambient electrons. Because the heat capacity of the ambient electrons is small the heat input from the photoelectrons would be expected to be equal to the total energy losses to the ions and neutral particles plus the downward heat conduction. These loss processes will be discussed in Section 9.



THEORETICAL HEAT INPUT TO AMBIENT
ELECTRONS FROM PHOTOELECTRONS
AND TOTAL MEASURED ENERGY LOSSES
OF AMBIENT ELECTRONS

FIGURE 23

8. ENERGY LOSSES OF THE CONJUGATE
POINT PHOTOELECTRONS DUE TO
EXCITATION OF OXYGEN RED LINE
IN THE DARK IONOSPHERE

There are several possible mechanisms for the excitation of the 6300 Å oxygen red line. Two of them will be considered in this work. Cole (1965) suggested that the hotter ambient electrons excited by the energetic incoming photoelectron from the sunlit conjugate region are responsible for the predawn enhancement of the oxygen red line. This mechanism will be considered in detail in Section 9. Another possible mechanism is the direct excitation of the oxygen red line by the incoming photoelectrons as suggested by Carlson (1966), and will be discussed in this section.

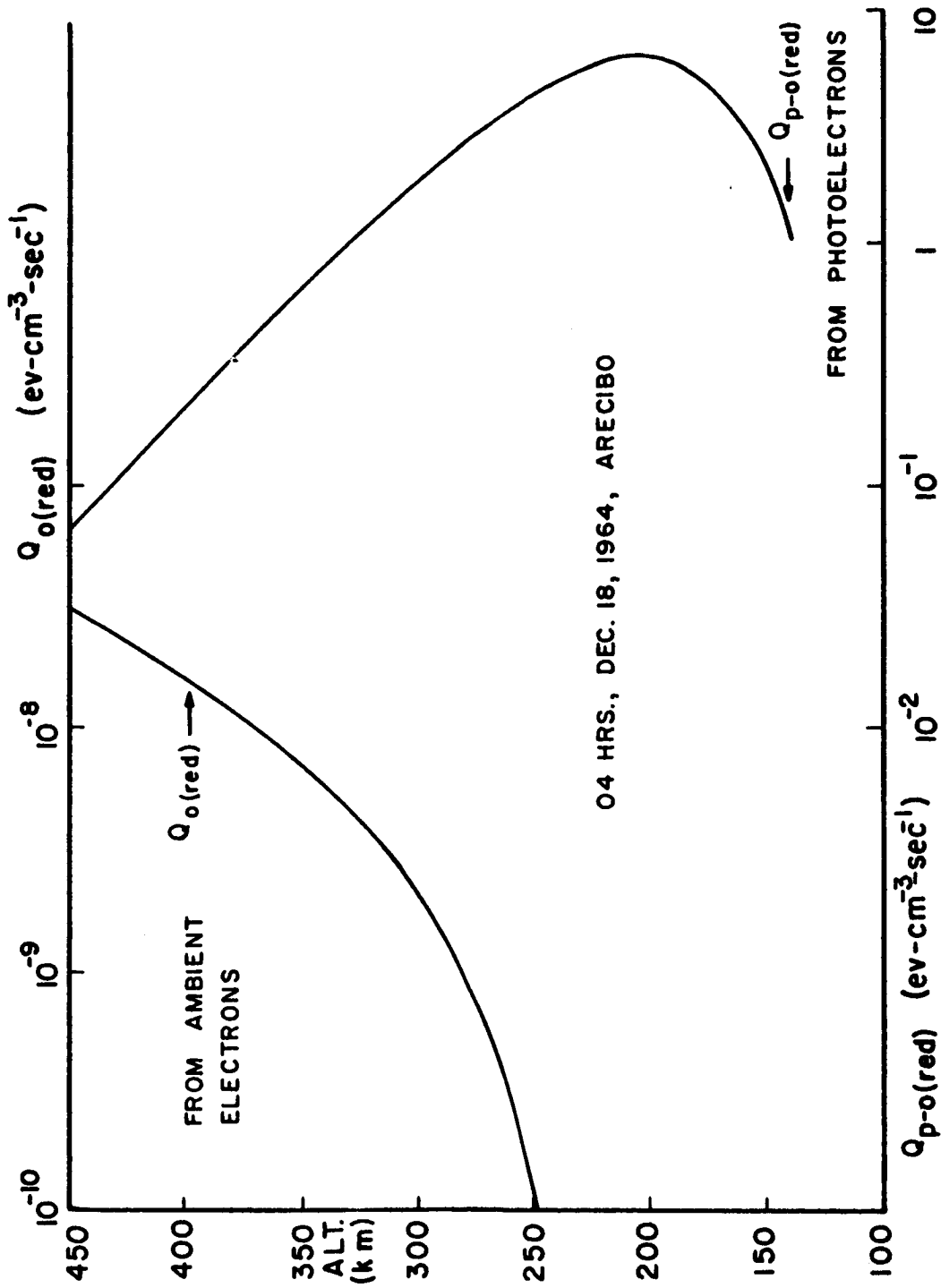
Upon their arrival at Arecibo the photoelectrons with energies greater than 2 eV are capable of exciting the oxygen red line. The energy loss of photoelectrons due to this process is given by

$$Q_{p-o(\text{red})} = \sum_{E=2\text{ev}}^{\infty} \frac{dE}{dx} \phi \quad (8.1)$$

where $\frac{dE}{dx}$ is the spatial rate of energy loss of a photoelectron, and ϕ is the photoelectron flux. Since the photoelectron loses 1.96 eV per collision with the atomic oxygen in exciting the 6300 Å red line, we have

$$Q_{p-o(\text{red})} = \sum_{E=2\text{ev}}^{\infty} \frac{2}{\lambda} \phi = \sum_{E=2\text{ev}}^{\infty} 2\sigma_r n(o) \phi \quad (8.2)$$

The calculated height profile of energy input for excitation of the oxygen red line is shown in Fig. 24. The emission peak at about 200 Km is due to the decrease of the photoelectron flux with decreasing altitude because of the collisions with the neutral particles according to Eq. (7.1), coupled with the number density of atomic oxygen increasing with decreasing altitude. The intensity of the oxygen red line is calculated to be about 44 Rayleighs. There were no experimental data available for the intensity of the oxygen line at Arecibo in December 1964 for comparison. However, the measured values of the intensity of the oxygen red line at Haute Provence during the predawn period near the winter solstice in 1953 (Barbier 1959) show a red line enhancement of about this value.



04 HRS., DEC. 18, 1964, ARECIBO

EXCITATION OF THE OXYGEN RED LINES (6300 Å)

FIGURE 24

9. ENERGY LOSSES OF AMBIENT ELECTRONS

9.1 Energy Loss Due to Excitation of 1D State of Atomic Oxygen

The excitations to the metastable 1D state of atomic oxygen by the incoming photoelectrons have been discussed in Section 8. The excitation by the ambient electrons will now be considered. At a certain electron temperature the ambient electrons in the high energy tail may have sufficient energy to excite the $[OI]$ red line ($6300 \overset{\circ}{\text{A}}$, $6364 \overset{\circ}{\text{A}}$). The loss rate of energy of ambient electrons for the red line excitation is given by (See Eq. (8.1)).

$$Q_{O(\text{red})} = \int_{2\text{ev}}^{\infty} \frac{dE}{dt} f(E) dE \quad (9.1.1)$$

where

$$\frac{dE}{dt} = v \frac{dE}{dx} = \sqrt{\frac{2E}{m_e}} 2 n(o) \sigma_r \quad (9.1.2)$$

since the excitation energy is 1.96 ev., and σ_r is the cross section for red line excitation. If the ambient electrons are distributed according to Maxwell's relation, then

$$f(V) dV = n_e \sqrt{\frac{2}{\pi} \left(\frac{m_e}{kT_e}\right)^3} v^2 e^{-\left(\frac{m_e v^2}{2kT_e}\right)} dV$$

where k is Boltzmann's constant, $f(V) dV$ is the number of electrons per cm^3 with speeds between V and $V + dV$, n_e is the number of electrons per cm^3 , T_e is the electron temperature in $^{\circ}\text{K}$, and m_e is the mass of an electron.

In terms of energy

$$f(E) dE = n_e \frac{2}{\sqrt{\pi}(kT_e)^{3/2}} e^{-\left(\frac{E}{kT_e}\right)} \sqrt{E} dE \quad (9.1.3)$$

The red line collision cross section curve as shown in Fig. 6 may be approximated by the following two equations:

$$\begin{aligned} \sigma_r &= 3.3 \times 10^{-7} \left(1 - e^{-\frac{E-2}{0.723}}\right) \text{ cm}^2, \quad 2 \leq E \leq 4.3 \text{ ev.} \\ \sigma_r &= 3.3 \times 10^{-17} e^{-\left(\frac{E-4.3}{12}\right)} \text{ cm}^2, \quad 4.3 \leq E \leq 15 \text{ ev.} \end{aligned} \quad (9.1.4)$$

Substituting Eq.s (9.1.2), (9.1.3), and (9.1.4) into Eq. (9.1.1) and upon integration, we have

$$Q_{o(\text{red})} = 3 \times 10^{-4} n_e n(o) T_e^{-\frac{1}{2}} e^{-\frac{2.3 \times 10^4}{T_e}} \left\{ 3.2 \times 10^{-3} + 1.37 \times 10^{-7} T_e - \frac{0.23}{72.5 + 8.65 \times 10^{-3} T_e} - \frac{72.8 \times 10^{-6} T_e}{525 + 0.125 T_e + 7.5 \times 10^{-6} T_e^2} \right\}$$

The calculated height profile of the energy input for excitation of red line due to ambient electrons is shown in Fig. 24. It is apparent that the excitation produced by the ambient electrons is very much less than that produced directly by the incoming photoelectrons. At 04 hrs., December 18, 1964, at the altitude of 300 Km. above Arecibo the electron temperature was about 800°K.

It is required that the electron temperature be as high as about 2000°K. to make a contribution to the excitation of the oxygen red line of $3\text{ev.}\cdot\text{cm.}^{-3}\cdot\text{sec.}^{-1}$ which is about that from the incident photoelectrons at the same altitude.

9.2 Energy Losses Due to Other Inelastic Collisions With the Neutral Particles

The rate of energy loss to molecular oxygen due primarily to collisional excitation of the rotational levels of O_2 , with a small contribution from excitation of vibrational states is given by

$$Q_{\text{O}_2(\text{rot. vib.})} = 1.31 \times 10^{-4} n_e n(\text{O}_2) \left\{ 4 \times 10^{-14} T_e - 8 \times 10^{-12} T_n \right\} \left\{ T_e - T_n \right\}$$

The coefficient has been taken from Hanson (1963).

The rate of heat loss due primarily to excitation of the rotational levels of N_2 is given by

$$Q_{\text{N}_2(\text{rot})} = 1.31 \times 10^{-4} n_e n(\text{N}_2) \left\{ 1.2 \times 10^{-11} - 5.6 \times 10^{-15} T_n \right\} \left\{ T_e - T_n \right\}$$

The coefficient has been obtained from Dalgarno and Moffett (1962).

9.3 Energy Losses Due to Elastic Collisions With Neutral Particles and Positive Ions

The elastic collisions with the neutrals and ions are also effective in cooling the electron gas. The loss rates of energy due to elastic collisions with the three primary constituents of the upper atmosphere (O , O_2 , N_2) have been

developed by Banks (1966) and adopted here.

$$Q_{0(\text{elastic})} = 3.74 \times 10^{-18} n_e n(O) T_e^{\frac{1}{2}} \left\{ T_e - T_n \right\}$$

$$Q_{O_2(\text{elastic})} = 1.21 \times 10^{-18} n_e n(O_2) \left\{ 1 + 3.6 \times 10^{-2} T_e^{\frac{1}{2}} \right\} T_e^{\frac{1}{2}} \left\{ T_e - T_n \right\}$$

$$Q_{N_2(\text{elastic})} = 1.77 \times 10^{-19} n_e n(N_2) \left\{ 1 - 1.21 \times 10^{-4} T_e \right\} T_e \left\{ T_e - T_n \right\}$$

and

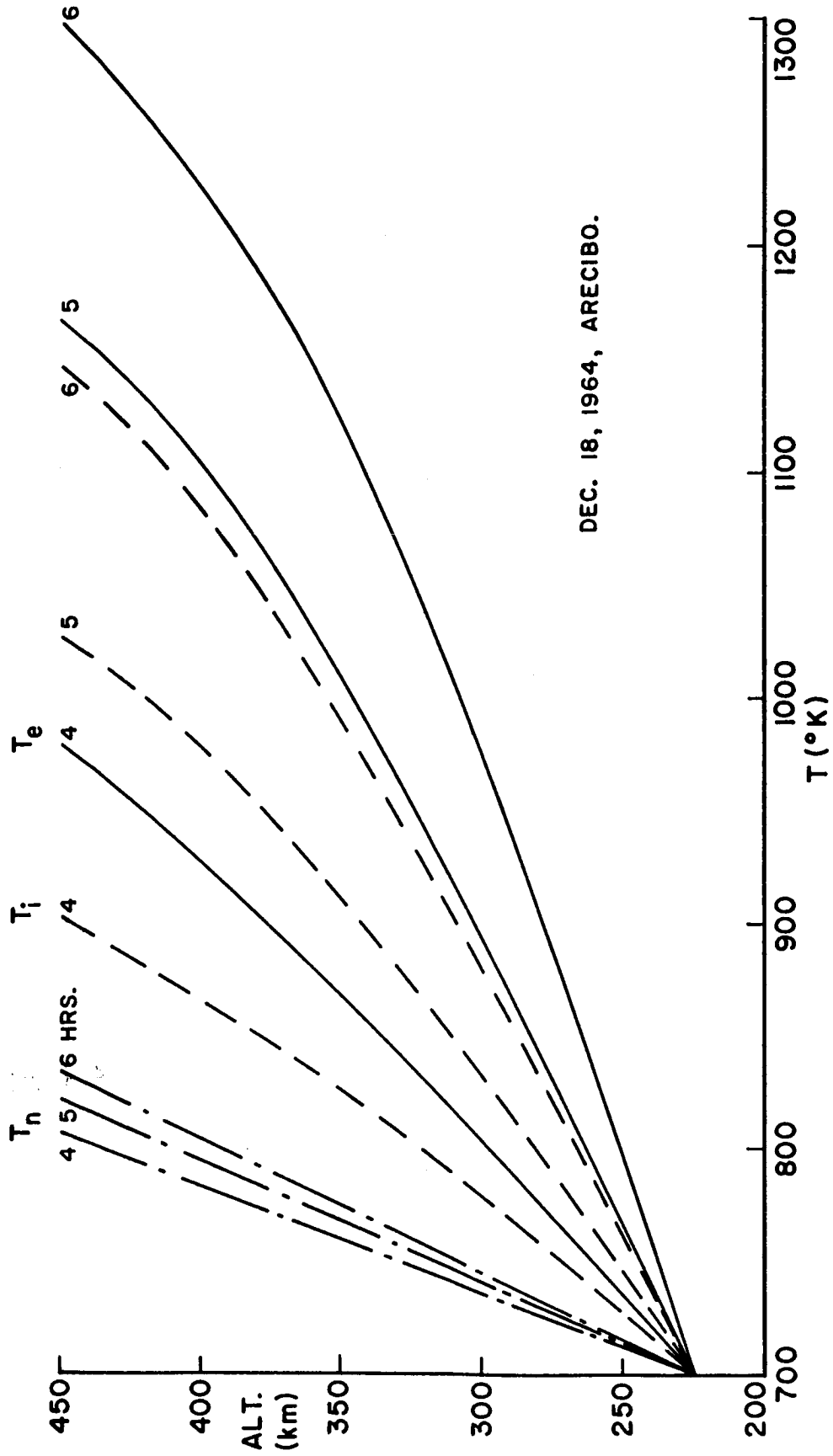
$$Q_{O^+} = 4.82 \times 10^{-7} n_e^2 T_e^{-\frac{3}{2}} \left\{ T_e - T_i \right\} \quad (\text{Hanson \& Johnson, 1961})$$

neglecting helium ion content at and below 400 Km. level.

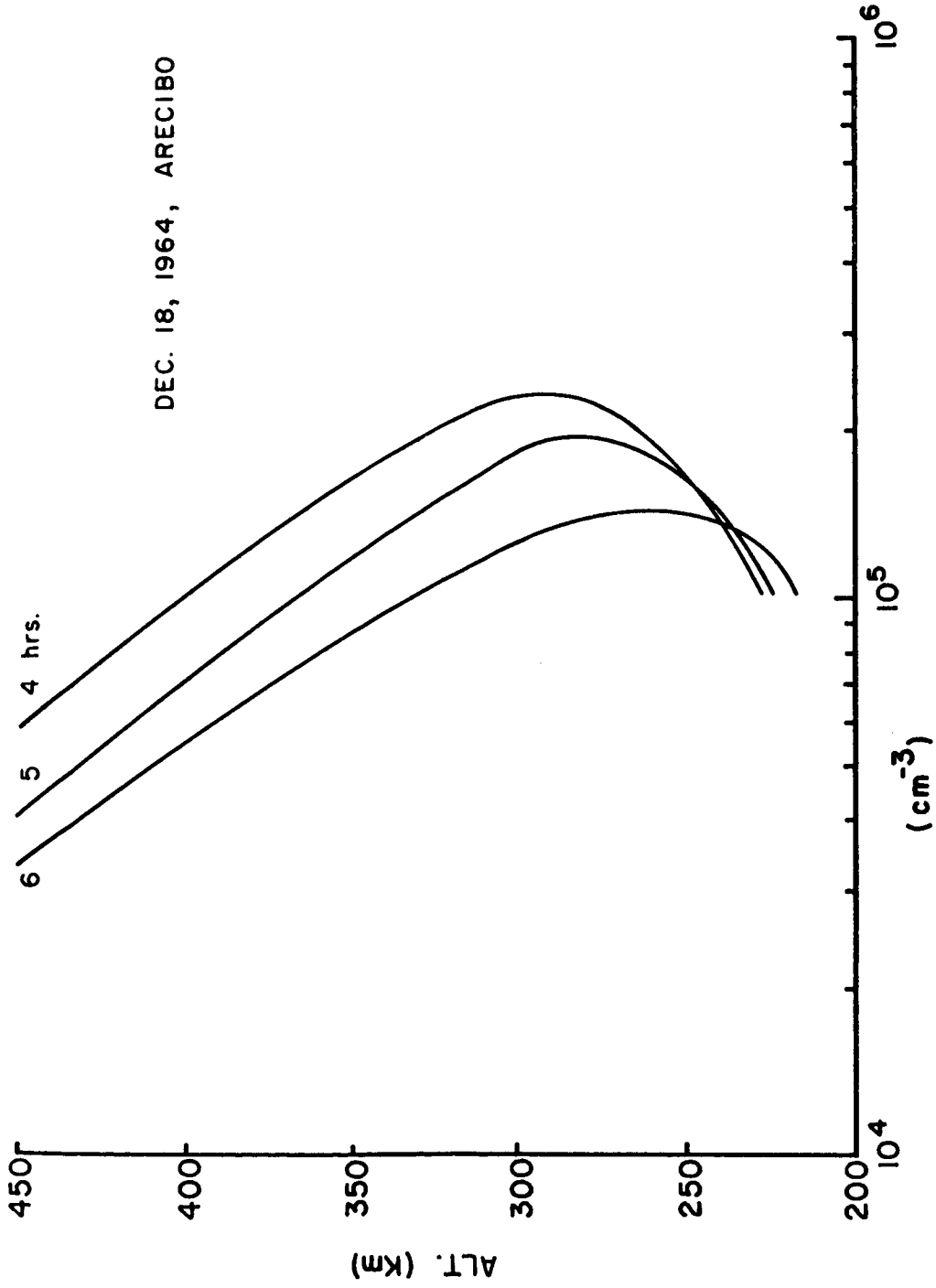
9.4 Height Profiles of Energy Losses of Ambient Electrons

The various energy losses of ambient electrons have been calculated using electron density, electron temperature and ion temperature observations made at the Arecibo Ionospheric Observatory on December 18, 1964 shown in Figs. 25 and 26.

Figs. 27 through 30 show the various energy losses of ambient electrons for three different hours in the early morning, while Fig. 31 illustrates the general behavior of the energy loss due to excitation of the red line. The energy loss through the collisional excitation of the red line is very sensitive to the electron temperature. It is obvious that this loss is negligible compared to other losses at this time. Fig. 27 also includes the thermal conduction of the ambient electrons to be discussed in Section 10.

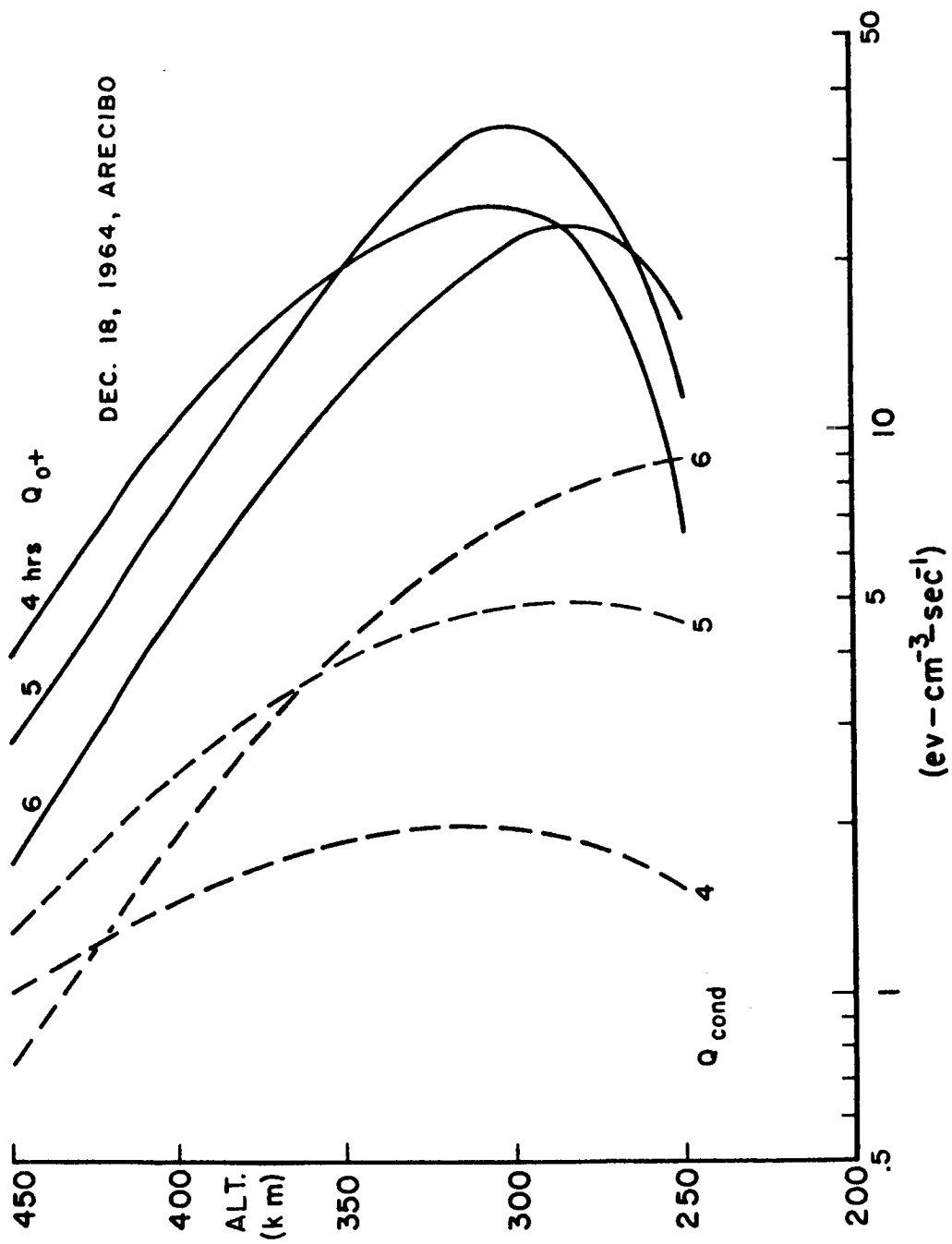


ELECTRON TEMPERATURE, ION TEMPERATURE AND NEUTRAL TEMPERATURE
FIGURE 25



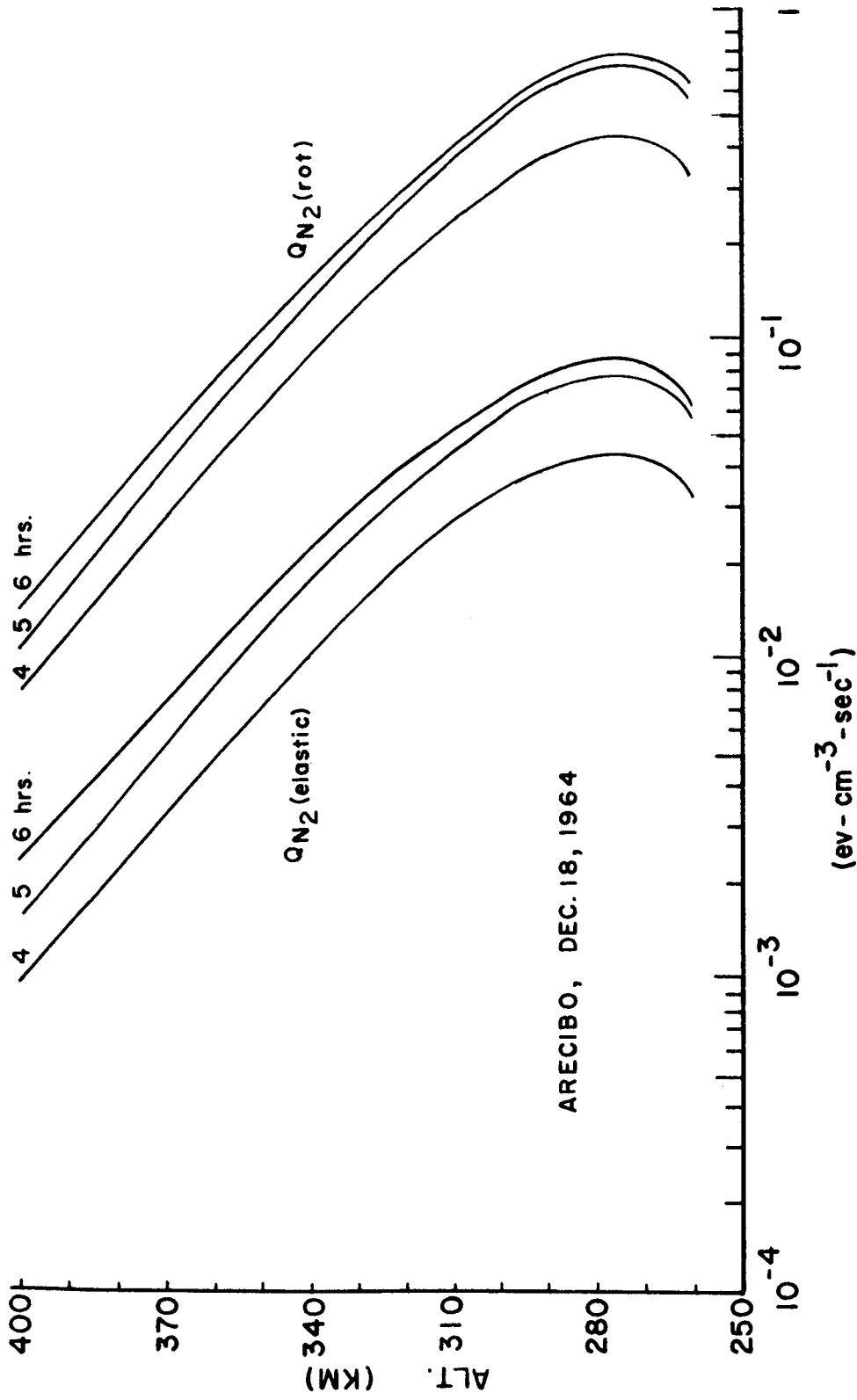
ELECTRON DENSITY

FIGURE 26



CONDUCTION AND ENERGY - LOSS OF AMBIENT ELECTRONS

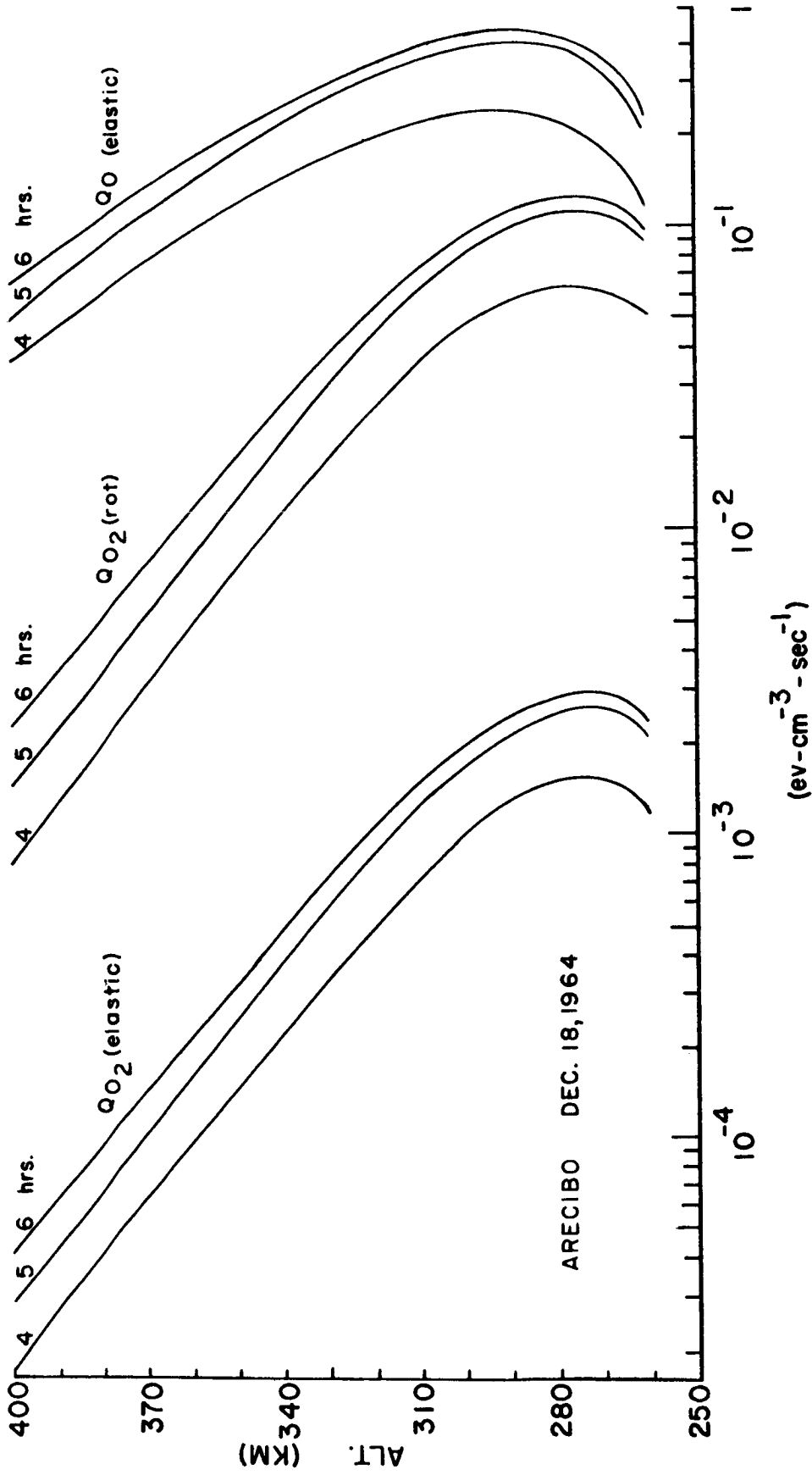
FIGURE 27



ARECIBO, DEC. 18, 1964

ENERGY-LOSS OF AMBIENT ELECTRONS

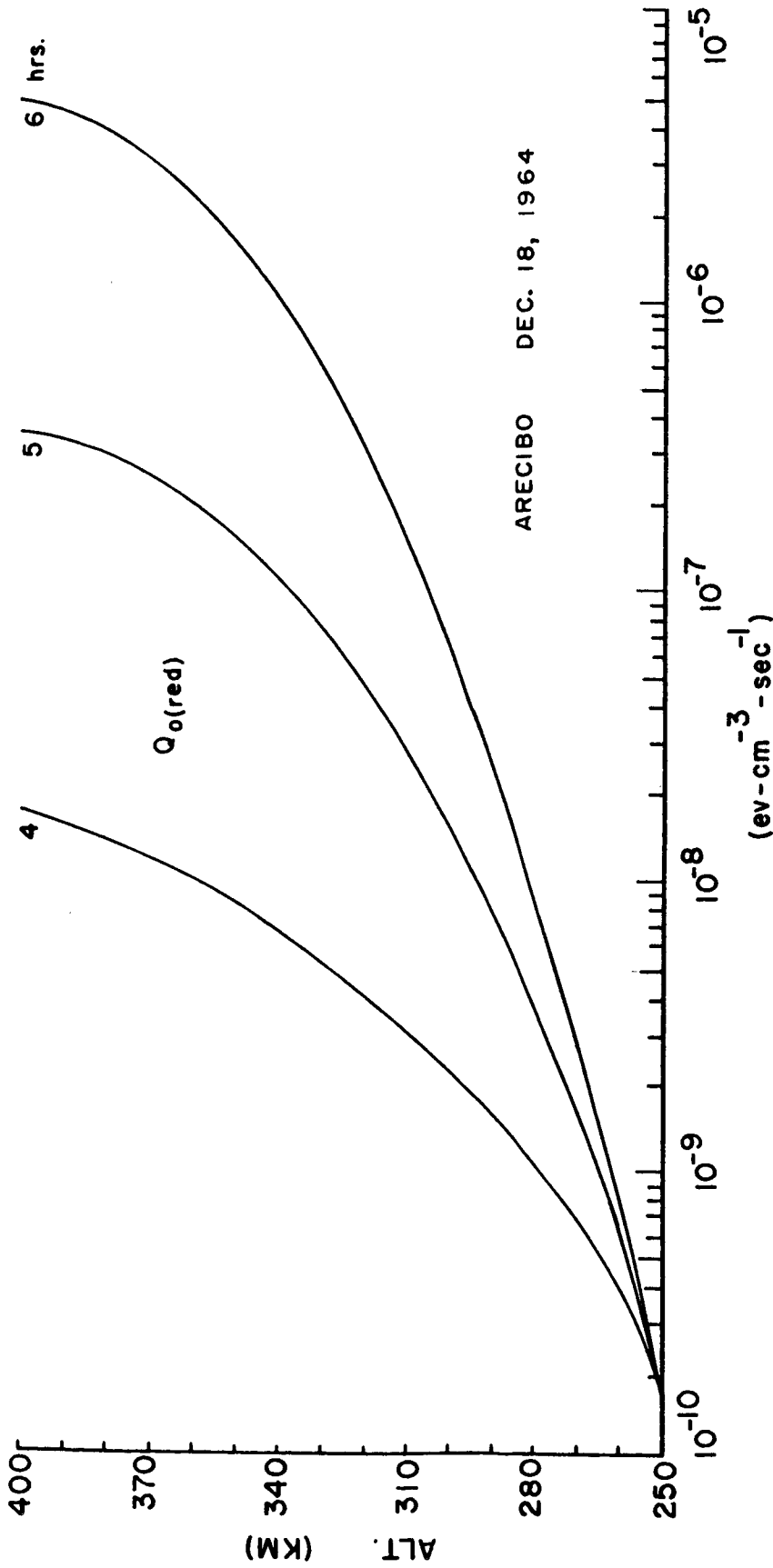
FIGURE 28



ARECIBO DEC. 18, 1964

ENERGY-LOSS OF AMBIENT ELECTRONS

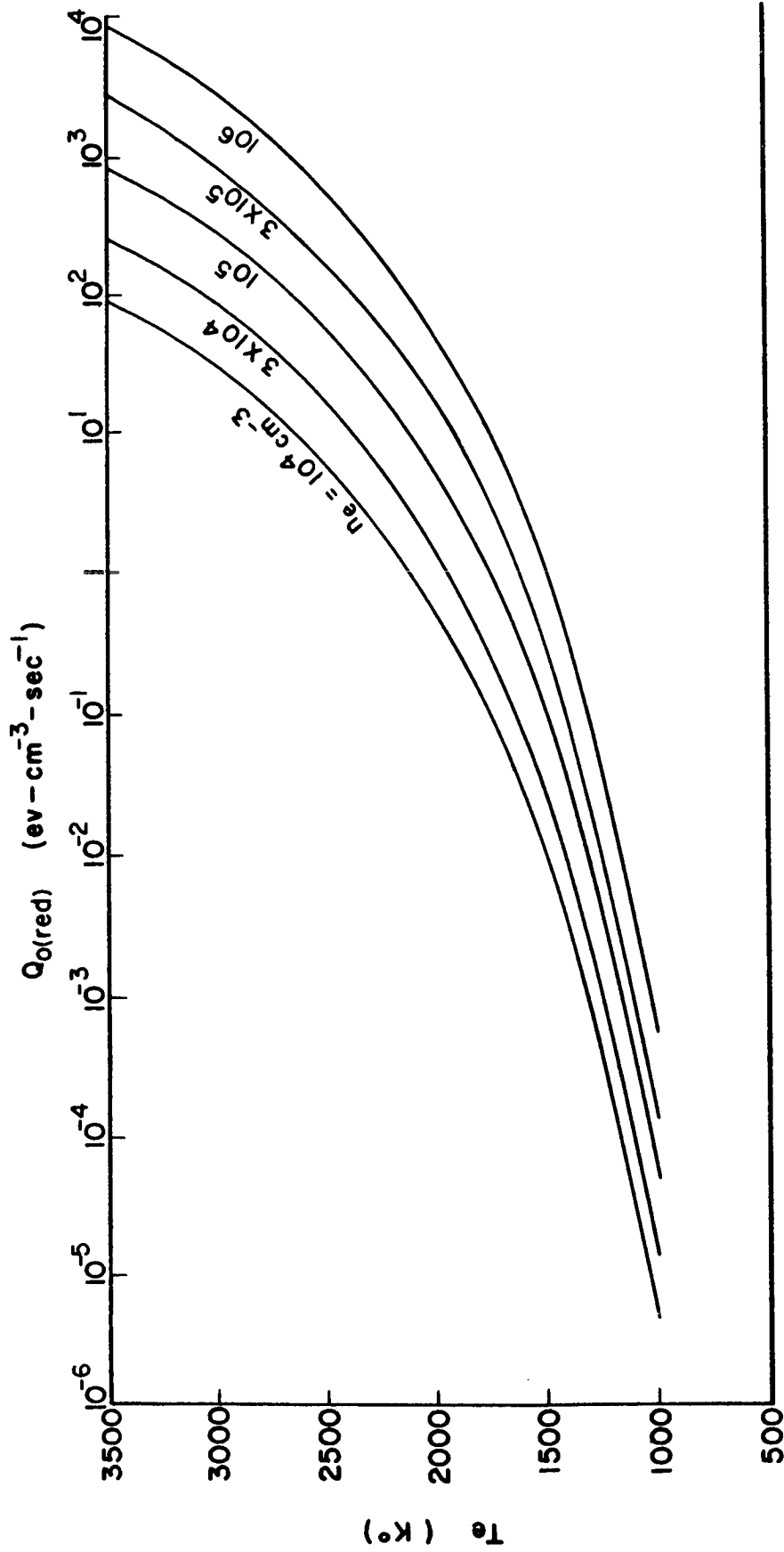
FIGURE 29



ARECIBO DEC. 18, 1964

ENERGY-LOSS OF AMBIENT ELECTRONS

FIGURE 30



ENERGY-LOSS OF AMBIENT ELECTRONS

FIGURE 31

10. THERMAL CONDUCTION

The thermal conductivity of a gas of charged particles is dependent upon the inverse square root of the mass of the particle (Chapman and Cowling, 1958; Spitzer, 1962). Thus, the thermal conductivity of the ion gas is small compared to that of the ambient electrons and thermal conduction by the ion gas may be neglected as a mechanism of heat transport. But the conduction by the ambient electrons may be comparable to the other energy losses and must be considered.

The ambient electron energy balance equation for steady state conditions between production, loss, and conduction may be written as

$$Q_i = Q_{\text{cond}} + Q_L'$$

where Q_i is the production rate of energy,

$$Q_{\text{cond}} = - \sin^2 I \frac{d}{dz} \left(K_e \frac{dT_e}{dz} \right)$$

and

$$Q_L' = Q_{O(\text{red})} + Q_{O(\text{elastic})} + Q_{N_2(\text{rot. vib.})} \\ + Q_{N_2(\text{elastic})} + Q_{O_2(\text{rot.})} + Q_{N_2(\text{rot. vib.})}$$

Using Eq. (6.1.5) for K_e the calculated conduction for three different hours is shown in Fig. 27 and is combined with Q_L' into Q_L for 04 hrs. in Fig. 23.

11. SUMMARY AND CONCLUSIONS

11.1 Energy Distribution of Photoelectron Number Density

The coupled continuity equations for the number densities of photoelectrons were solved by assuming steady state and neglecting the divergence term but taking into account the probability of escape of a photoelectron.

The calculated number densities of photoelectrons are comparable in magnitude to those computed by Hoegy et al. (1965) up to 300 Km. who assumed that all photoelectrons are localized. This is as would be expected because our calculations showed the divergence of the photoelectron flux to be small and the probability of escape of a photoelectron is small in this region.

For energies less than about 13 ev. the gradients of number density of photoelectrons are large below about 300 Km. compared to those above this altitude.

Up to about 30 ev. the number density of photoelectrons is generally decreasing with increasing altitude above the 260 Km. level, but above 30 ev. it is practically independent of the altitude.

11.2 Diffusion Flux and Escape Flux of Photoelectrons

The diffusion flux of photoelectrons was calculated using the number density of photoelectrons under the condition that the divergence of the diffusion flux of photoelectrons is neglected. The diffusion flux of photoelectrons was found to be of the order of 10^7 electrons-

$\text{cm}^2\text{-sec}^{-1}$ for the altitude range 280-320 Km. and for energies up to about 20 ev. Although the diffusion flux of photoelectrons is quite large, the divergence of the diffusion flux of photoelectrons was found to be small in general compared to the total production term and total loss term in the continuity equation, and the original assumption made in solving the continuity equations for the number density of photoelectrons is justified.

The escape flux of photoelectrons was found to depend on the number of elastic collisions per second with the neutral particles as well as the probability of escape of a photoelectron without further collision. The calculated escape flux of photoelectrons is comparable in magnitude to the diffusion flux of photoelectrons at the 300-Km level.

11.3 Energy Deposited in the Protonosphere and the Downward Heat Flux

The energy transferred to the ambient electrons along the field line in the protonosphere due to elastic collisions with the photoelectrons spiralling up from the conjugate region was calculated. The heat flux so deposited above 1000 Km. was found to be about 1×10^9 ev.-cm.⁻²-sec.⁻¹. One half of this was assumed to conduct downwards at the Arecibo end of the field line which agrees fairly well with the reasonable extrapolation of the calculated heat flux at Arecibo. Difficulties in interpretation of the measurement of temperature when the relative densities of atomic oxygen, helium and hydrogen

ions are varying make such heat conduction measurements uncertain above 450 Km. for these observations.

11.4 Heat Input and Energy-Loss of the Ambient Electrons in the Dark Ionosphere Above Arecibo

The height profile of heat input to the ambient electrons in the ionosphere above Arecibo at 04 hrs. 60^oW., December 18, 1964 due to both the incident photoelectrons and the thermal conduction of the ambient electrons along the field line was calculated and compared very well with the height profile of the total energy losses of the ambient electrons both in shape and magnitude. The heat input is controlled mainly by the flux of photoelectrons with energies below about 10 ev.

11.5 Predawn Enhancement of the Intensity of 6300 Å^o Airglow Red Line

The energy required to excite the oxygen red line was calculated. The attenuation of the incoming photoelectron flux below 300 Km. due to collisions with neutral particles has been taken into account. The integrated emission rate was found to be about 44 Rayleighs which checks closely with the predawn values of about 50 Rayleighs measured by Barbier at Haute Provence near winter solstice in 1953. The significance of this comparison is in the indication it provides of the total photoelectron flux above 2 ev. Estimates by Nisbet (1967) make it appear that the general flux and attenuation assumptions used for the Arecibo calculations should be comparable to those at Haute Provence.

11.6 Suggestions for Further Research

In the present analysis the photoelectron fluxes and the effect they have in increasing the electron temperature in the conjugate region and exciting the airglow have been calculated for low sunspot conditions at Arecibo, Puerto Rico. Further measurements and calculations are desirable at other locations and other times in the sunspot cycle.

The present study utilized spectral measurements using 500 micro second pulses. This severely limited the vertical resolution of the electron temperature measurements. New equipment and techniques are available using a double pulse correlation method which allows simultaneous measurements to be made at several altitudes with very much greater altitude resolution. In addition the correlation technique allows the determination of the autocorrelation functions unperturbed by pulse width effects. In this way much more reliable measurements can be made, not only of the electron and ion temperatures but also of the relative concentrations of the ionic constituents in the lower ionosphere. This would be desirable in allowing the comparison of the theoretical and observed temperature to be extended to lower altitudes.

This study has indicated that the heat conducted downward through the 1000 Km. level both during the pre-dawn period and during the day is a useful indicator of

the photoelectron flux in the protonosphere. It would therefore be desirable to conduct a series of measurements throughout the solar cycle and to examine the measurements of others to determine these temperature gradients and hence the flux conducted downwards for comparison with theoretical estimates of the photoelectron flux.

The present study has investigated the intensity of the 6300 Å airglow line at Arecibo under low sunspot conditions. While measurements have been made at Arecibo and other stations of the intensity of the 6300 Å airglow line on the ground it would be very desirable to supplement these with a series of rocket measurements of the 6300 Å airglow line during the pre-sunrise period as a function of altitude. This would provide valuable information not only on the total photoelectron flux but also on its energy spectrum.

Bibliography

- Banks, P. M., Energy transfer and charged particle temperatures in the upper atmosphere, Ph.D. Thesis, Pennsylvania State University, University Park, Pa., 1965.
- Banks, P. M., Collision frequencies and energy transfer-electrons, Scientific Report No. 271, Ionosphere Research Laboratory, Pennsylvania State University, University Park, Pa., 1966.
- Banks, P. M., Collision frequency and energy transfer: electrons, Planetary Space Sci., 14, 1085-1104, 1966.
- Barbier, D., Recherches sur la raie 6300 de la luminescence atmospherique nocturne, Annales de Geophys. 15, 179-217, 1959.
- Boksenberg, A., Electron collision processes in dissociated molecular bases, Ph.D. Thesis, University of London, 1961.
- Brace, L. H., B. M. Reddy, Latitudinal variations of electron temperature and concentration from satellite probes, presented at the COSPAR Sixth International Space Science Symposium, Buenos Aires, Argentina, May 13-19, 1965.
- Brode, R. B., The quantitative study of the collisions of electrons with atoms, Rev. Mod. Phys. 5, 257-279, 1933.
- Butler, S. J., and M. J. Buckingham, Energy loss of a fast ion in a plasma, Phys. Rev., 126, 1-4, 1962.
- Carlson, H. C., and J. S. Nisbet, Electron densities and temperatures in the F-region from backscatter measurements at Arecibo, presented at the NATO Advanced Study Institute on Electron density profiles in the ionosphere and exosphere, Finse, Norway, April, 1965.
- Carlson, H. C., Ionospheric heating by magnetic conjugate point photoelectrons as observed at Arecibo, Ph.D. Thesis, Cornell University, Ithaca, N. Y., 1966.
- Carlson, H. C., Ionospheric heating by magnetic conjugate-point photoelectrons, J. Geophys. Res. 71, 195-199, 1966.

- Carlson, H. C., Conjugate point heating observed at Arecibo, Conference on Thomson Scatter Studies of the Ionosphere, University of Illinois, April 10-12, 1967. Unpublished communication.
- Carru, H., M. Petit, and P. Waldteufel, Observation by incoherent scatter of the heating of the ionosphere by photoelectrons from the magnetic conjugate point, Cospar 1966.
- Chapman, S., The absorption and dissociative or ionizing effect of monochromatic radiation in an atmosphere on a rotating earth, Proc. Phys. Soc. 43, 484-501, 1931.
- Chapman, S., and T. G. Cowling, The Mathematic Theory of Non-Uniform Gases, Cambridge University Press, 1958.
- CIRA 1965 Cospar International Reference Atmosphere 1965, Compiled by Working Group IV. COSPAR, published by North-Holland Publishing Company-Amsterdam.
- Cole, K. D., The predawn enhancement of 6300 Å ⁰airglow, Annales de Geophys. 21, 156-158, 1965.
- Dalgarno, A., Charge particles in the upper atmosphere, Annales de Geophys. 17, 16-34, 1961.
- Dalgarno, A., and R. J. Moffett, Electron cooling in the D-region, Planetary Space Sci., 9, 439-441, 1962.
- Dalgarno, A., M. B. McElroy, and R. J. Moffett, Electron temperatures in the ionosphere, Planetary Space Sci., 11, 463-484, 1963.
- Engelhardt, A. G., A. V. Phelps, and C. G. Risk, Determination of momentum transfer and inelastic collision cross-sections for electrons in nitrogen using transport coefficients, Phys. Rev., 138, A 1566-A 1574, 1964.
- Evans, J. V., Ionospheric backscatter observations at millstone hill, Planetary Space Sci., 13, 1031-1074, 1965.
- Evans, J. V., Photoelectron escape flux determinations at millstone hill, Conference on Thomson Scatter Studies of the Ionosphere, University of Illinois, April 10-12, 1967. Unpublished Communication.

- Farley, D. T., Observations of the equatorial ionosphere using incoherent backscatter, presented at the NATO Advanced Study Institute on electron density profiles in the ionosphere and exosphere, Finse, Norway, April 1965.
- Fite, W. L., and R. T. Brackmann, Ionization of atomic oxygen on electron impact, Phys. Rev. 113, 815-816, 1959.
- Geisler, J. E., and S. A. Bowhill, An investigation of ionosphere-protonosphere coupling, Aeronomy Report No. 5, Aeronomy Laboratory, University of Illinois, Urbana, Ill., 1965.
- Hanson, W. B., and F. S. Johnson, Electron temperatures in the ionosphere, Memoires Soc. R. Liege, IV, 390-423, 1961.
- Hanson, W. B., Electron temperature in the upper atmosphere, Space Res., 3, 282-302, 1963.
- Hinteregger, H. E., L. A. Hall, and G. Schmidtke, Solar XUV radiation and neutral particle distribution in July 1963 thermosphere, Space Res., 5, 1175-1190, 1965.
- Hoegy, W. F., J. P. Fournier, and E. G. Fontheim, Photoelectron energy distribution in the F-region, J. Geophys. Res. 70, 5464-5468, 1965.
- Mariani, F., Photoionization rates in a time variable atmosphere: diurnal, latitudinal and solar cycle variations, Goddard Space Flight Center Preliminary Report, 1964.
- McDaniel, E. W., Collision Phenomena in Ionized Gases, Wiley, New York, 1964.
- Mitra, S. K., The Upper Atmosphere, The Asiatic Society, Calcutta, Second Edition, 1952.
- Nicolet, M., Dynamic effects in the high atmosphere, in The Earth as a Planet, edited by G. P. Kuiper, University of Chicago Press, 1954.
- Nisbet, J. S., Photoelectrons escape from the ionosphere and fluxes in the conjugate hemisphere, presented to the 1967 Conjugate Point International Symposium, June 13-16, Boulder, Colorado.

- Perkins, Jr., F. W., Two problems in the kinetic theory of plasmas: Propagation of a test particle in a plasma and the spectrum of electron-density fluctuations for a non-Maxwellian electron gas, Res. Rep. RS. 58, Cornell University, Ithaca, N. Y., 1964.
- Perkins, F. W., and E. E. Salpeter, Enhancement of plasma density fluctuations by non-thermal electrons, Phys. Rev., 139, A55-A62, 1965.
- Perkins, F. W., E. E. Salpeter, and K. O. Yngvesson, Incoherent scatter from plasma oscillations in the ionosphere, Phys. Rev. Letters, 14, 579-581, 1965.
- Quinn, T. P., and J. S. Nisbet, The recombination coefficient of the nighttime F layer, J. Geophys. Res., 68, 1031-1038, 1963.
- Rapp, D., P. Englander-Golden, Total cross-sections for ionization of atoms and molecules by electron impact, Lockheed Missiles and Space Co, Report No. 6-74-64-12, 1965.
- Schulz, G. J., and J. T. Dowell, Excitation of vibrational and electronic levels in O₂ by electron impact, Phys. Rev., 128, 174-177, 1962.
- Seaton, M. J., Airglow and Aurorae, Pergamon Press: London, Eds. E. B. Armstrong and A. Dalgarno, 1956.
- Spitzer, L., Physics of Fully Ionized Gases, Interscience Publishers, 1962.
- Stewart, D. T., Electron excitation functions of the first negative bands of N₂⁺, Proc. Phys. Soc. A, 69, 437-440, 1956.
- Stewart, D. T., and E. Gabathuler, Some electron collision cross section for nitrogen and oxygen, Proc. Phys. Soc., 72, 287-289, 1958.
- Sunshine, G., B. B. Aubrey, and B. Bederson, Absolute measurements of total cross-sections for the scattering of low-energy electrons by atomic and molecular oxygen, Department of Physics, New York University, 1966.
- Swider, W., The ionic structure of the ionosphere, Ph.D. Thesis, Pennsylvania State University, University Park, Pa., 1963.

Takao Tohmatsu, Toshihiro Ogawa and Haruo Tsuruta, Photo-electronic processes in the upper atmosphere, I energy spectrum of the primary photoelectrons, Report of Ionosphere and Space Research in Japan, 18, 482-508, 1965.

APPENDIX

The optical depth is (for the terrestrial atmosphere consisting of O, O₂, and N₂)

$$\sum_i \tau_i = \tau(O) + \tau(O_2) + \tau(N_2) \quad (A1)$$

$$\tau(O) = K_A(O) \int_0^\infty n(O) dl \quad (A2)$$

$$\tau(O_2) = K_A(O_2) \int_0^\infty n(O_2) dl \quad (A3)$$

$$\tau(N_2) = K_A(N_2) \int_0^\infty n(N_2) dl \quad (A4)$$

where K_{Ai} = absorption cross section

$$N_{ih} = \int_0^\infty n_i dl = \text{total number of particles of } i\text{th constituent per cm}^2 \text{ column along some optical path } l \text{ in the ionosphere above a certain altitude } h.$$

For an overhead sun, $\chi = 0$, and constant scale height H ,

$$N_{ih} = n_{ih} H_{ih} = n_{ih} H_i, \quad H_{ih} = H_i = \text{constant.}$$

The optical depth factor is defined as:

$$F_i = \frac{N_{ih}(\chi \neq 0)}{N_{ih}(\chi = 0)} = \frac{\int_0^\infty n_i dl}{n_{ih} H_i} = \frac{\tau_{ih}}{n_{ih} H_i K_{Ai}} > 1 \quad (A5)$$

$F_i = \sec \chi$ for a flat earth and constant scale height.

$$N_{ih} = \int_0^\infty n_i dl = n_{ih} H_i F_i \quad (A6)$$

$$q_{ih} = n_{ih} K_{Ii} \Phi_\infty e^{-\sum_i K_{Ai} n_{ih} H_i F_i} \quad (A7)$$

Hence the total production rate at a given height h is

$$q = q(O) + q(N_2) + q(O_2) \quad (A8)$$

$$q = \sum_{i=1}^3 \sum_{\lambda} n_i K_{Ii} \Phi_{\infty} e^{-\sum_{i=1}^3 K_{Ai} n_i H_i F_i} \quad (A9)$$

$$[I] \quad \underline{\chi \leq \frac{\pi}{2}}$$

(A) The determination of the optical depth factor for a constant scale height atmosphere on a spherical earth was given by Chapman (1931)

$$F_o = \frac{\int_0^{\infty} n dl}{n_h H} = \frac{\int_0^{\infty} n_h e^{-\frac{Z}{H}} dl}{n_h H} \quad (A10)$$

after some manipulations and with $X = \frac{a+n}{H}$

$$F_o = ch(X, \chi) = X \sin \chi \int_0^{\chi} \left[\exp X \left(1 - \frac{\sin \chi}{\sin \alpha} \right) \right] \csc^2 \alpha d\alpha \quad (A11)$$

This is called the Chapman function which is difficult to compute; Wilkes (1954) has done so using a digital computer.

(B) For a constant scale-height gradient atmosphere other functions can be derived. The scale height gradient is defined as the rate of change of H in the vertical direction $\beta = dH/dZ$. If β is constant, the neutral density is approximately represented by (Nicolet 1954)

$$n(z) = n_h \left(\frac{H}{H_h} \right)^{-\left(\frac{1+\beta}{\beta} \right)} \quad (A12)$$

The optical depth factor for a constant β atmosphere is given by

$$F_\beta(X, \chi, \beta) = \frac{1}{n_h H_h} \int_0^\infty n dl = \frac{1}{n_h H_h} \int_0^\infty n_h \left(\frac{H}{H_h} \right)^{-\left(\frac{1+\beta}{\beta} \right)} dl \quad (A13)$$

after some manipulations the following equation (Swider, 1963) may be obtained:

$$F_{\frac{1}{2}}(\beta = \frac{1}{2}, X, \chi) = \frac{1}{G^2 (\sin^2 \chi - d^2)} \left[3 \left(\frac{\sin^2 \chi}{\sin^2 \chi - d^2} \right) - 1 \right] \left[1 - G \cos \chi \right] \\ - \frac{d \cos \chi}{\sin^2 \chi - d^2} + \frac{6 d \sin^2 \chi}{G^2 (\sin^2 \chi - d^2) (|\sin^2 \chi - d^2|)^{3/2}} \\ \left[\coth^{-1} \left(\sqrt{\frac{d}{|\sin^2 \chi - d^2|}} \right) + \coth^{-1} \left(\sqrt{\frac{\frac{1}{G} - \cos \chi}{|\sin^2 \chi - d^2|}} \right) \right] \quad (A14)$$

replacing \coth^{-1} with \tan^{-1} when $\sin \chi > d$, where

$$G = \frac{a+h}{2H_h}, \quad d = 1 - \frac{1}{G}.$$

$$F_1(\beta=1, X, \chi) = \frac{m}{m^2 - \sin^2 \chi} \left[\cos \chi - \frac{1}{X} \right] + \frac{2 \sin^2 \chi}{X \sqrt{|m^2 - \sin^2 \chi|}^3} \\ \left\{ \coth^{-1} \left(\sqrt{\frac{m}{|m^2 - \sin^2 \chi|}} \right) - \coth^{-1} \left(\sqrt{\frac{\cos \chi - \frac{1}{X}}{|m^2 - \sin^2 \chi|}} \right) \right\} \quad (A15)$$

replacing \coth^{-1} with \tan^{-1} when $\sin \chi > m$, where

$$X = \frac{a+h}{H_h}, \text{ and } m = 1 - \frac{1}{X}.$$

Swider calculated F_1 and F_1 and compared values of $\sec \chi$, F_0 , F_1 , and F_1 for various X values and values of χ ranging from 70° to 90° . The values of F_0 are those calculated by Wilkes (1954). From the table in Swider's thesis it can be seen that for a given X , $\sec \chi > F_0 > F_1 > F_1$. The values of $\sec \chi$ are quite different from those of F_0 , F_1 , and F_1 when $\chi > 80^\circ$ and at high altitudes, so $\sec \chi$ should be replaced by the approximate function in these regions. Otherwise, the production rate of photoelectrons would be too small.

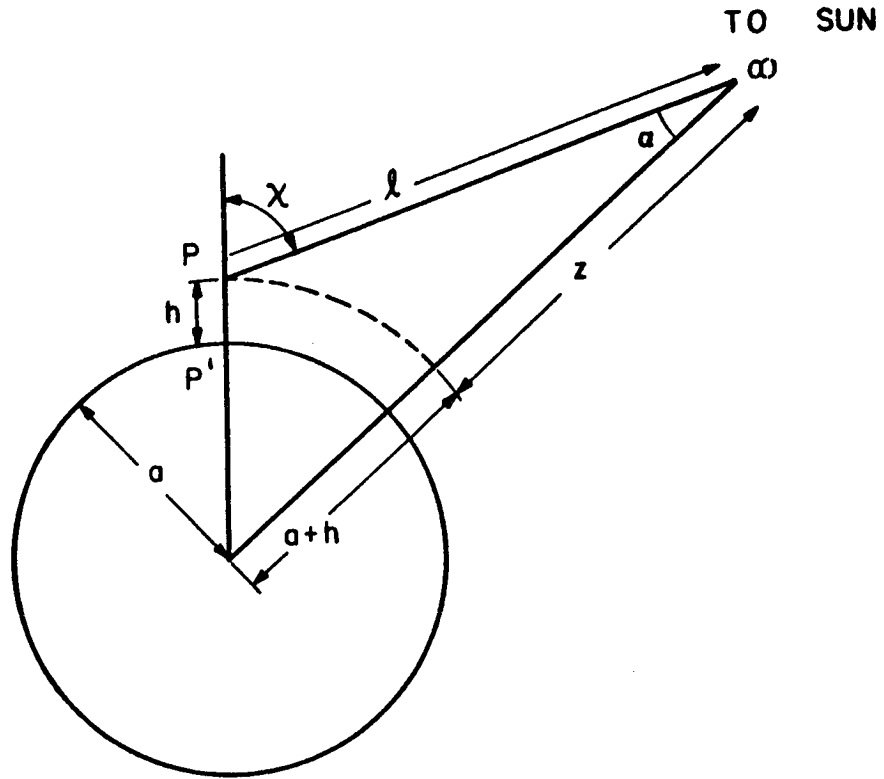
$$\underline{[II] \quad \chi = \frac{\pi}{2}}$$

Nicolet (1945) has shown that it is possible to use a simple approximation for the optical depth factor when $\chi = \frac{\pi}{2}$, namely:

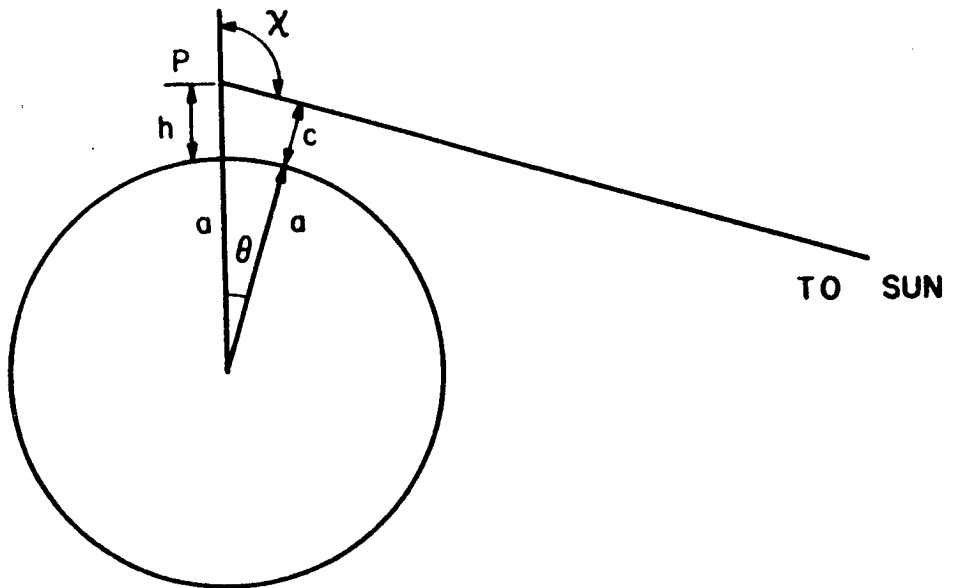
$$F \left(\chi = \frac{\pi}{2}, \theta = 0 \right) = \sqrt{\frac{\pi}{2} \left(\frac{a+c}{H_c} \right)}, \quad \theta = \chi - \frac{\pi}{2} \quad (A16)$$

$$\text{and } \mathcal{T} = n_c H_c K_A F = n_c H_c K_A \sqrt{\frac{\pi}{2} \left(\frac{a+c}{H_c} \right)} \quad (A17)$$

This approximation is good if the scale height is constant and compares very closely with the Chapman function $Ch(\chi = 90^\circ)$. For the major part of the optical depth,



THE GEOMETRY FOR $\chi < \pi/2$
FIGURE A1



THE GEOMETRY FOR $\chi \geq \pi/2$
FIGURE A2

the local scale height is not too different from H_c .

$$\underline{[III]} \quad \chi > \frac{\pi}{2}$$

In this case the Nicolet function F_N is an excellent approximation.

$$F_N = \sqrt{\frac{\pi}{2}} \frac{a+c}{H_c} \left[1 + \operatorname{erf} \sqrt{\left(\frac{a+c}{H_c}\right) (\sec \theta - 1)} \right] \quad (A18)$$

where erf denotes the error function. The corresponding optical depth is $\tau = n_c H_c K_A F_N$. The equation for c (the distance of closest approach of the solar ray to the earth's surface) may be derived from Fig. A2.

$$\frac{c+a}{h+a} = \cos \theta = \frac{1}{\sec \theta} \quad (A19)$$

$$c = \frac{h-a (\sec \theta - 1)}{\sec \theta}, \quad \theta = \chi - \frac{\pi}{2} \quad (A20)$$

For an $O - O_2 - N_2$ atmosphere, the production of atomic oxygen is

$$q_h(0) = n_h(0) K_I(0) \Phi_{\infty} e^{-[\tau(0) + \tau(O_2) + \tau(N_2)]} \quad (A21)$$

where

$$\tau(0) = n_c(0) H_c(0) K_A(0) F_N(h, c, \theta, H_c(0)) \quad (A22)$$

$$\tau(O_2) = n_c(O_2) H_c(O_2) K_A(O_2) F_N(h, c, \theta, H_c(O_2)) \quad (A23)$$

$$\tau(N_2) = n_c(N_2) H_c(N_2) K_A(N_2) F_N(h, c, \theta, H_c(N_2)) \quad (A24)$$

Similarly, we can find $q_h(O_2)$ and $q_h(N_2)$.

ACKNOWLEDGMENTS

This work was supported in part under NASA Grant NsG 134-61.

The author is grateful to the staff of the Arecibo Ionospheric Observatory and of the Ionosphere Research Laboratory of The Pennsylvania State University for obtaining the data. The Arecibo Ionospheric Observatory is operated by Cornell University with the support of the Advanced Research Projects Agency under a research contract with the Air Force of Scientific Research.